International
Progress Report

IPR-02-44

Äspö Hard Rock Laboratory

Dynamic changes of groundwater flow and geochemical distribution during tunnel construction

Task 5. Modelling impact of the tunnel construction on the groundwater system at Äspö, a hydrogeological–hydrochemical model assessment exercise

Takuma Hasegawa
Yasuharu Tanaka
Yasunori Mahara
Toshifumi Igarashi

Abiko Research Laboratory, Central Research Institute of Electric Power Industry (CRIEPI)

November 2001

Svensk Kärnbränslehantering AB
Swedish Nuclear Fuel
and Waste Management Co
Box 5864
SE-102 40 Stockholm Sweden
Tel +46 8 459 84 00
Fax +46 8 661 57 19

Äspö Hard Rock
Laboratory

Report no.	No.
IPR-02-44	F65K
Author	Date
Hasegawa, Tanaka, Mahara, Igarashi	01-11-01
Checked by	Date
Hasegawa	01-11-30
Approved	Date
Christer Svemar	02-11-19

Äspö Hard Rock Laboratory

Dynamic changes of groundwater flow and geochemical distribution during tunnel construction

Task 5. Modelling impact of the tunnel construction on the groundwater system at Äspö, a hydrogeological–hydrochemical model assessment exercise

Takuma Hasegawa
Yasuharu Tanaka
Yasunori Mahara
Toshifumi Igarashi

Abiko Research Laboratory, Central Research Institute of Electric Power Industry (CRIEPI)

November 2001

Keywords: Groundwater flow, solute transport, coupled hydrogeochemistry, Äspö, Task 5

Executive summary

The groundwater flow and geochemical distribution were simulated during tunnel construction around Äspö. The stability of selected geochemical components was investigated using PHREEQE.

An unsteady state of groundwater flow was simulated by considering the progress of the tunnel and the change of inflow to the tunnel section. Excluding modelling the grouting and skin effect around tunnel, the measured inflows at the weir were assigned to the tunnel sections as the flux boundary. Calibrations of the transmissivity of the Hydraulic Conductor Domains (HCDs) were also performed.

The progress of tunnel construction and the time series of drawdowns are quite useful to understand the hydrogeological model because these relationships clarify the impact and response. Drawdowns were roughly represented by properly representing the geometric relationship between tunnel, shaft, HCDs and monitoring borehole section.

The geochemical distribution of selected chemical components was simulated using the results of the Multivariate Mixing Mass balance calculations (M3). The simulated mixing proportions of old waters (i.e. Glacial water and Brine water) and the sum total of fresh water mixing proportions (i.e. sum total of Baltic Sea water and Meteoric water) agreed with the results of M3, but the ratio of fresh water (i.e. Baltic Sea water and Meteoric water) did not. Based on the simulated mixing proportions, the deeper part of the groundwater was replaced by Baltic Sea water rather than Meteoric water. Furthermore, based on PHREEQE calculations, some geochemical components are sensitive to geochemical reactions.

Further studies are needed to explain some of the inconsistencies identified, for example, the role of geochemical reactions, the influence of boundary conditions, the local effects of sampling etc. However, use of the end-members helps to understand the groundwater flow-paths and the properties of the HCDs.

Concerning helium concentrations, the simulated helium concentrations are generally in good agreement with the measured concentrations. Since measured and simulated results reflect the hydraulic properties of the HCDs, it is a potentially useful method to verify the hydrogeological model.

Sammanfattning

Grundvattenflöde och geokemisk distribution simulerades under tunneldrivning på Äspö. Stabiliteten hos valda geokemiska komponenter undersöktes me hjälp av PHREEQE.

Ett oregelbundet grundvattenflöde simulerades genom beaktande av tunnelns framdrivning och förändringen av inflöde till tunnelsektionen. Utan att modellera sattes injektering, skinnzonen runt tunneln, det uppmätta inflödet och vattenvallarna som flödesränder i tunnelsektionerna. Kalibrering av transmissiviteten hos de hydrauliska ledarnas domäner (Hydraulic Conductor Domain - HCD) gjordes också.

Tunnels framåtskridande och tidsserierna för avsänkningen är mycket användbara för förståelsen av den hydrogeologiska modellen, eftersom dessa förhållanden klargör påverkan och reaktion. Avsänkningarna representerades grovt av en korrekt representation av geometriskt förhållande mellan tunnel, schakt, HCDer och monitering av borrhålssektioner.

Den geokemiska distributionen av valda kemiska komponenter simulerades med hjälp av resultaten från beräkningar med Multivariate, Mixing och Mass balance (M3). Den simulerade blandningsproportionen av gammalt vatten (dvs. glacialvatten och saltvatten) och totalsumman av sötvattnets blandningsproportioner (dvs. summan av Östersjövatten och meteoriskt vatten) överensstämde med resultaten från M3, men kvoten sött vatten (dvs. summa av Östersjövatten och meteoriskt vatten) stämde inte. De simulerade blandningsproportionerna indikerar att den djupare delen av grundvattnet ersatts av Östersjövatten snarare än meteoriskt vatten. Vidare har PHREEQE-beräkningar visat att vissa geokemiska komponenter är känsliga mot geokemiska reaktioner.

Ytterligare studier krävs för att förklara vissa av de identifierade oklarheterna, t ex geokemiska reaktioners roll, randvillkorens påverkan, den lokala påverkan av provtagning etc. Användningen av slutprodukter hjälper dock till med att förstå grundvattnets flödesvägar och HCDernas egenskaper.

Beträffande heliumkoncentrationerna stämmer i allmänhet de simulerade heliumkoncentrationerna väl överens med de uppmätta koncentrationerna. Eftersom uppmätta och simulerade resultat återspeglar HCDernas hydrauliska egenskaper är detta en potentiellt användbar metod för att verifiera den hydrauliska modellen.

Table of Contents

Executive summary ..... **i**

Sammanfattning ..... **iii**

1. Introduction **1**

1.1 Background 1
1.2 Objectives 1

2. Description of modelling site **3**

2.1 Overview 3
2.2 Geological and hydrogeological models 3
2.3 Geochemical distribution 4
2.3.1 End members 4
2.3.2 Conservative solutes 5
2.3.3 Helium (^{4}He) 7

3. Modelling tools **9**

3.1 Numerical model 9
3.2 Groundwater flow 9
3.3 Solute transport 9
3.4 Main features of FEGM-B 10
3.4.1 Element 10
3.4.2 Matrix solver 10
3.4.3 Smeared fracture model 11

4. Modelling assumptions **13**

4.1 Modelling area 13
4.2 Boundary conditions of groundwater flow 14
4.3 Initial and boundary conditions of geochemical distribution 15
4.4 Simulated conditions 15
4.5 Data used 15
4.5.1 Hydraulic conductivity 15
4.5.2 Specific storage 17
4.5.3 Effective flow porosity 18
4.5.4 Dispersion 18

5. Simulated results and discussion **19**

5.1 Groundwater flow 19
5.1.1 The features of measured drawdowns 19
5.1.2 Calibration 22
5.1.3 The simulated drawdowns 27
5.2 Geochemical conditions 29
5.2.1 Changes in geochemical distribution 29
5.2.2 Expected groundwater flow to control point 30
5.2.3 The simulated geochemical distribution 30

6. Helium concentration 35
6.1 Background 35
6.2 Main features of helium 35
6.3 Model description 35
6.4 Calculated results 36
7. Geochemical reactions 39
7.1 Background 39
7.2 Modelling process 39
7.3 Geochemical reactions considered 41
7.4 Assumptions 41
7.5 Geochemical reaction analysis 42
7.6 Calculated results 45
8. Main results 49
Acknowledgements 51
References 53
Appendix 1: Questionnaire 55

1. Introduction

1.1 Background

The scenario of released radionuclides from engineered barriers to the biosphere along the groundwater flow pathways is critical to the execution of high-level radioactive waste disposal. Therefore it is important to evaluate the stability of groundwater flow for a long period of time (thousands to hundreds of thousands of years). However, because of the difficulties in verifying the long-term stability, the utilisation of a wide variety of methods is required.
The Äspö Hard Rock Laboratory (HRL) test site was constructed by the Swedish Nuclear Fuel and Waste Management Co. (SKB) near Oskarshamn, southeastern Sweden, to investigate high-level waste disposal in a deep geological formation. Several international groups are participating in collaborative projects. One of these projects, Task 5, is concerned with the integration of hydrodynamics with hydrochemistry to investigate the changes in the groundwater system during tunnel construction. In this report, the consistency between geochemical and hydrogeological modelling during the Äspö tunnel construction is described and discussed.

1.2 Objectives

The principle objectives defined in this task are to check the consistency between groundwater flow and geochemical distribution and to develop the procedure of evaluating groundwater flow systems. Thus, CRIEPI applied the FEGM-B code for groundwater flow and solute transport to the change of groundwater flow during tunnel construction at Äspö and to integrate the simulated results of groundwater flow with the geochemical data evaluation by using the PHREEQE code. This code identifies the potential effect of equilibrium geochemical reactions on the groundwater chemistry.

2. Description of modelling site

2.1 Overview

The Äspö HRL consists of a spiral tunnel and a series of niches. The tunnel starts on the mainland at Simpevarp and two spirals under Äspö island reach a depth of 450 m with a total length of 3600 m. Tunnel construction started in October 1990 and was completed in September 1995. Construction was by two methods; blasting from the entrance to a distance of 3200 m, and by TBM for the final 400 m.

Prior to tunnel construction, geological, hydrogeological and hydrochemical investigations using boreholes to depths around 800-900 m were conducted to characterise the site for groundwater flow and geochemical distribution. Following tunnel construction, groundwater flow and geochemical monitoring has been conducted not only in these boreholes, but also from boreholes in the tunnel.

2.2 Geological and hydrogeological models

Äspö belongs to the Trans-Scandinavian Granite-Porphyry Belt and the main rock types at the site comprise Äspö diorite, Småland granite, greenstones and fine-grained granites. It is estimated by the U-Pb method that these rocks were formed around 1800 Ma ago. With respect to structures, on a regional scale the most dominating features are trending NS, EW and NW, whilst at the scale of the Äspö site a NE-ENE trending structure dominates. These structures are also considered to have been formed some 1800 Ma ago.

These structures have high transmissivities and constitute the Hydraulic Conductor Domains (HCDs). Therefore they are sensitive to the groundwater flow and solute transport of the region.

In order to evaluate the groundwater flow and solute transport around Äspö it is important to identify the HCDs. So far, 17 HCDs have been identified at Äspö ranging in hydraulic conductivity from 10^{-4} to 10^{-6} m/s. The remaining hydraulic domain, the so-called Hydraulic Rock mass Domain (HRD), is in the order of 10^{-9} m/s.

The average rainfall and evaporation rates are around 700 mm/y and 590 mm/y, respectively. Considering the surface run off, an infiltration rate of lower than 100 mm/y is expected.

When the tunnel intersects a HCD, a very high inflow rate can be expected. Consequently, grouting was performed to prevent high inflow into the tunnel during construction. The inflow rate to the tunnel is measured at weirs located every 150 m along the tunnel.

2.3 Geochemical distribution

2.3.1 End members

Since Äspö is an island in the Baltic Sea, the geochemical component of shallow groundwater is influenced by that of the Baltic Sea in addition to meteoric recharge water. From a palaeohydrochemical point of view, components of older marine water, ancient deep-seated brines and younger Quaternary glacial water are all present in varying proportions. Using the M3 approach, Laaksoharju (1999) categorised the Äspö groundwater as comprising a mixture of four major end members: Äspö Brine, Glacial, Meteoric and Baltic Sea waters. The results of the M3 principle component analysis performed by Gurban et al. (1998) and the distribution of the end-members are shown in Figures 1 and 2, respectively. The figures show that the older water components, Äspö Brine and Glacial, characterise the deeper groundwater, and that the younger Meteoric and Baltic Sea waters tend to dominate at shallower levels.

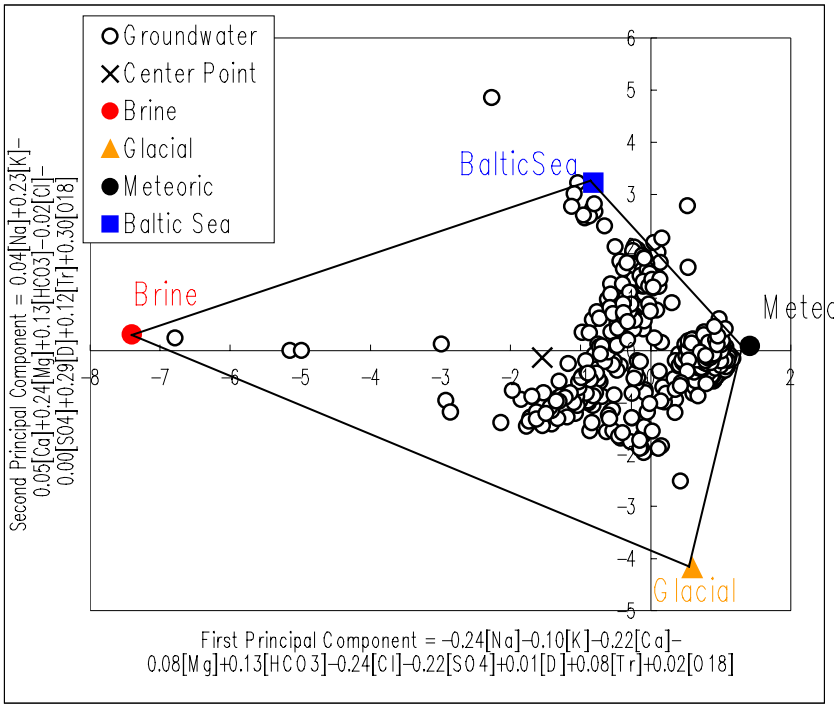

Figure 1*.PCA plot used as a basis for the M3 calculations.*
(from Gurban et al. (1998))

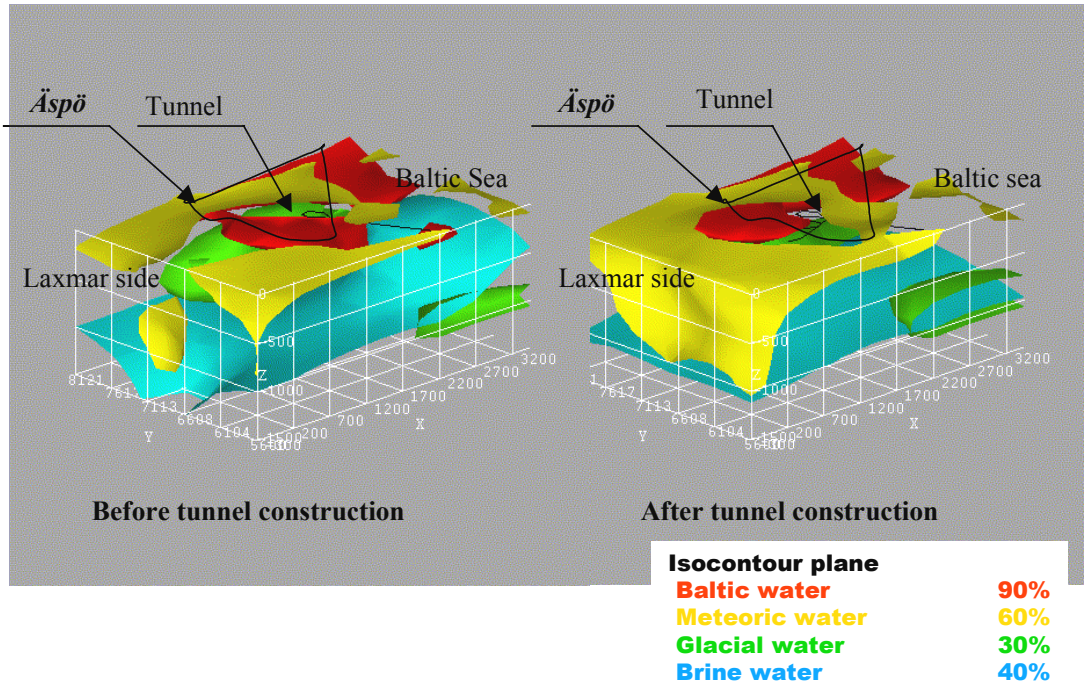

Figure 2. *3D distribution of end members before and after tunnel construction. (Each colour of iso-contour plane shows the mixing proportions of end members in right lower legend.)*

2.3.2 Conservative solutes

Chloride and $\delta^{18}O$ are the two major conservative solutes (Figure 3). The chloride concentration has been influenced by palaeoevents and increases with depth such that its concentration exceeds that of the Baltic Sea. The Baltic Sea and fresh water interface occurs at around 200 m depth under Äspö.

The distribution of $\delta^{18}O$ is affected by a number of glacial events during the Quaternary period. As a result of these events, low $\delta^{18}O$ values characterise the Laxemar and deeper levels of Äspö.

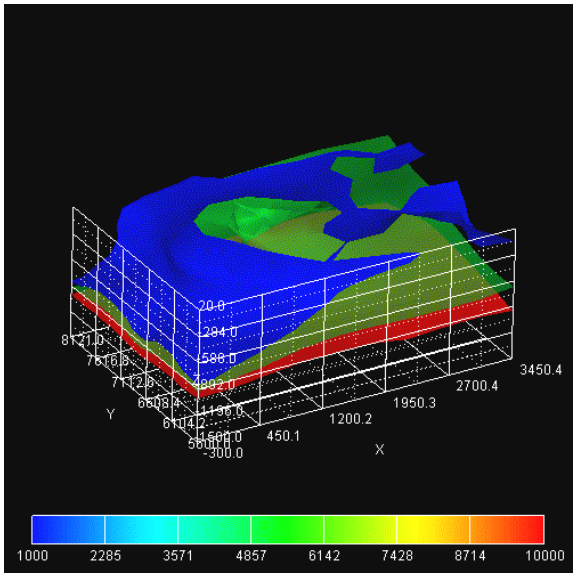

(1) Choloride concentration

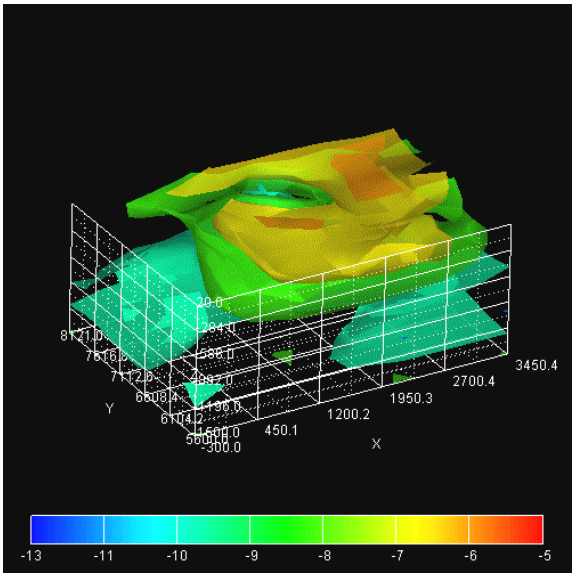

(2) $\delta^{18}O$

Figure 3. *Conservative solute distribution around Äspö before tunnel construction. (Planes show the iso-contour plane for each solute.)*

2.3.3 Helium (^{4}He)

Helium (^{4}He) is produced by the radioactive decay of uranium and thorium and accumulates in the rock and soil. Therefore, helium concentrations will be higher where the groundwater is stagnant. Mahara et al. (2000) investigated the ^{4}He concentrations in 1995 and 1997 in the tunnel (Figure 4). The concentration of the ^{4}He corresponded to the retention time of groundwater: stagnant zone, mixing zone and intrusion zone of Baltic Sea water. The zones estimated by ^{4}He concentration were located non-uniformly, allowing the effect of differing hydraulic conductivities of the rock mass to be estimated.

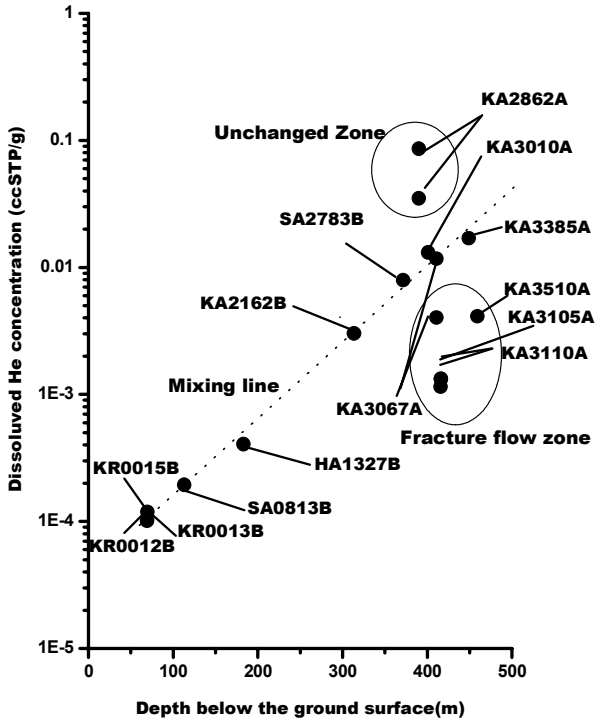

Figure 4. *Correlation between the dissolved helium content and the sampling depth in the tunnel. These are categorised into three zones: mixing, unchanged and fracture flow zone.*

3. Modelling tools

3.1 Numerical model

This section provides the description of the modelling tool applied to Task 5. The FEGM-B code which is a coupled code between FEGM (Kawanishi et al, 1994) and FERM (Kawanishi et al, 1995) was used. The FEGM and FERM are numerical codes for simulating groundwater flow and solute transport respectively, both of which are based on the Galerkin finite element method. These codes were developed by CRIEPI.

3.2 Groundwater flow

The equation of groundwater flow is described by the continuum equation and Darcy's law. Darcy's law is expanded to consider the density effect by using the Boussenesq approximation. These equations are discrete to a finite element.

The FEGM-B code can deal with a saturated-unsaturated seepage flow, and handle non-linear boundary conditions, for example, seepage face boundaries, rain infiltration boundaries and time-dependent boundaries.

The continuum equation of groundwater flow is as follows:

$$\left(\theta\beta'+\frac{\theta}{\phi}\alpha'+\frac{\partial\theta}{\partial h}\right)\frac{\partial h}{\partial t}+\frac{\partial}{\partial x_i}V_i+Q=0\,. \tag{1}$$

Darcy's law is as follows:

$$V_i=-k_r\cdot K\frac{\partial H_D}{\partial x_i}=-k_r\cdot K\left(\frac{\partial h}{\partial x_i}+\frac{\rho}{\rho_0}\frac{\partial z}{\partial x_i}\right) \tag{2}$$

$$H_D=h+\frac{1}{\rho_0}\int\rho dz\approx h+\frac{\rho}{\rho_0}z \tag{3}$$

Where t: time, x: coordinate, V_i: Darcy's velocity, Q: sink/source term, θ: volumetric water content, α': compressibility of media, β': compressibility of water, ø: porosity, K: hydraulic conductivity tensor, k_r: relative permeability, H_D: hydraulic head, h: pressure head, ρ: density, ρ_o: density of reference water , z: vertical coordinate

3.3 Solute transport

The governing equation of solute transport is described by the advection-dispersion equation. This equation can evaluate the movement of reactive tracers considering the retardation factor. This equation is discrete to a finite element in a similar fashion to the groundwater flow.

The governing equation of solute transport is as follows:

$$(\theta + \rho_b K_d)\frac{\partial}{\partial t}C + \left\{\frac{\partial \theta}{\partial t} + \alpha(\theta + \rho_b K_d)\frac{\partial h}{\partial t}\right\}C - \frac{\partial}{\partial x_i}\theta D_{ij}\frac{\partial}{\partial x_j}C + \frac{\partial}{\partial x_i}V_i C + M = 0 \quad (4)$$

Dispersion tensor is expressed as follows,

$$\theta D_{ij} = \alpha_T |V|\delta_{ij} + (\alpha_L - \alpha_T)\frac{V_i V_j}{|V|} + D_m \tau\theta\delta_{ij} \quad (5)$$

where C: concentration, ρ_b: bulk density, K_d: distribution coefficient, V_i: Darcy's velocity, α: solid compressibility, θ: volumetric water content, h: pressure head, α_L: longitudinal dispersion length, α_T: transverse dispersion length, |V|: absolute velocity, D_m: molecular diffusion, τ: tortuosity, M: source term.

Numerical calculation of solute transport has some difficulties relating to high peclet numbers. Therefore this code has a function known as the up-winding method, called streamline up-winding (Brooks and Hughes, 1982). Based on this method the weighting function changes the shape function to the following function:

Weighting function of streamline up-winding,

$$W^T = N^T + \frac{\tilde{\alpha} h_l}{2}\frac{\partial N^T}{\partial x_i}\frac{V_i}{|V|} \quad (6)$$

Where W^T: weighting function, N^T: shape function, α: cell peclet number, h_l: representative length of element, V_i: velocity, |V|: absolute velocity.

3.4 Main features of FEGM-B

3.4.1 Element

The FEGM-B can handle the following elements:

- One-dimensional: line
- Two-dimensional: triangle, square
- One-dimensional: tetrahedron, hexahedron, triangular prism

3.4.2 Matrix solver

This code can solve matrix equation as listed in Table 1. The direct method is unsuitable for the large matrix. This kind of problem, e.g. three-dimensional model, is ordinarily solved by the GMRES.

Table 1: Available matrix solver in FEGM-B

Direct method	Band Matrix Method	Gauss Elimination
	Block Skyline Method	LU Decomposition (Crout method)
Interactive method	CG	Conjugate Gradient Method
	BCG	Bi- Conjugate Gradient Method
	CGS	Conjugate Gradient Squared Method
	GMRES	Generalized Minimal Residual Method

3.4.3 Smeared fracture model

In order to treat fractures in a simple manner, FEGM-B incorporates a smeared fracture model that integrates the property of the fracture into finite elements by the volume-weighted method. When the fracture intersects several finite elements as shown in Figure 5, the parameters of the shadowed finite elements change to a volume weighted average values.

In order to simplify the explanation, a two-dimensional flow field as shown in Figure 5 is presumed. A single fracture is crossing a square element. The groundwater flows only in the direction parallel to a fracture surface in a fracture. Accordingly the hydraulic conductivity tensor of the fracture, $\boldsymbol{k}_f$', in a coordinate (x', y') is expressed by the following equation.

$$\boldsymbol{k}_f{}' = \begin{pmatrix} k^f_{x'x'} & 0 \\ 0 & 0 \end{pmatrix}$$

The hydraulic conductivity tensor of the fracture could transform the local coordinate ($\boldsymbol{k}_f$') to a global coordinate as follows,

$$\boldsymbol{k}_f = \begin{pmatrix} k^f_{x'x'} \cdot \cos^2\theta & k^f_{x'x'} \cdot \sin\theta \cdot \cos\theta \\ k^f_{x'x'} \cdot \sin\theta \cdot \cos\theta & k^f_{x'x'} \cdot \sin^2\theta \end{pmatrix}$$

Where θ is the angle of the axis x with the axis x'.

The hydraulic conductivity tensor of the element, $\boldsymbol{k}_e$, in a coordinate (x, y) is expressed as the following equation

$$\mathbf{k}_e = \frac{\mathbf{k}_f \cdot V_f + \mathbf{k}_m \cdot V_m}{V_e}$$

Where $\boldsymbol{k}_m$ is the hydraulic conductivity tensor of the rock matrix in a coordinate (x, y), V_e is the area of the element, V_f is the area of the fracture in the element, and V_m is the area of the rock matrix in the element.

In this study, this smeared fracture model was used to model the HCDs.

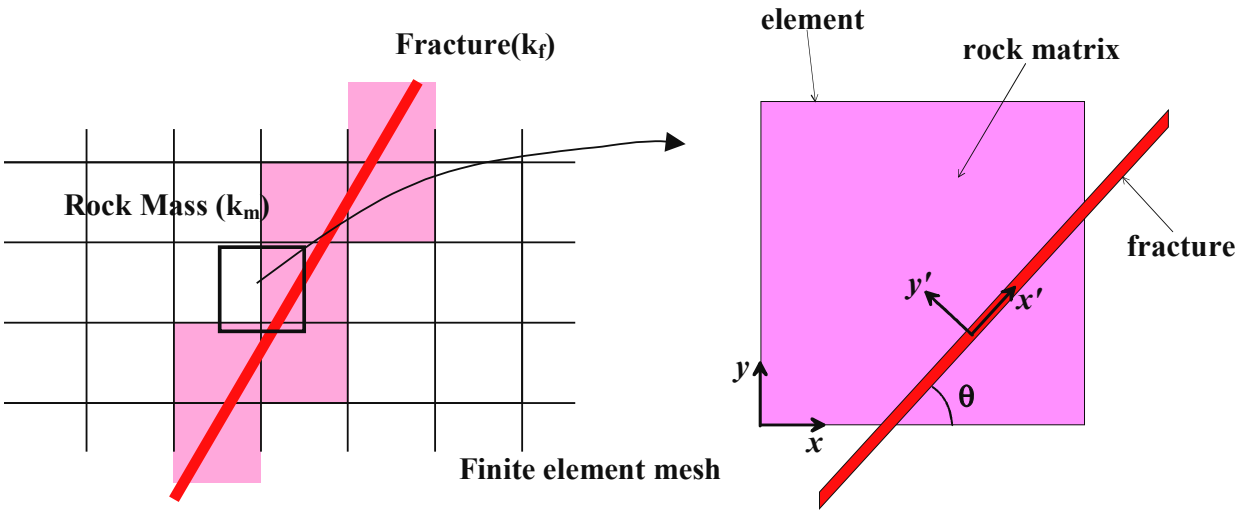

Figure 5. *Concept of smeared fracture model. The properties of the finite elements intersected by the fracture are calculated using the volume-weighted method.*

4. Modelling assumptions

4.1 Modelling area

In this study the groundwater flow and geochemical distribution were simulated around Äspö during tunnel construction. Therefore, the modelling area needs to cover the tunnel and the general Äspö area. To exclude the boundary effect, modelling was carried out in the range of 1000 to 3000 m easting, 5500 to 8000 m northing and 0 to -1000 m in depth within the Äspö coordinate system.

The finite elements around the tunnel were divided finely and the tunnel and elevator shaft were modelled by line elements. The modelling area and finite element diagram are shown in Figure 6. The HCDs are modelled by the smeared fracture model and it was not shown in finite element diagrams.

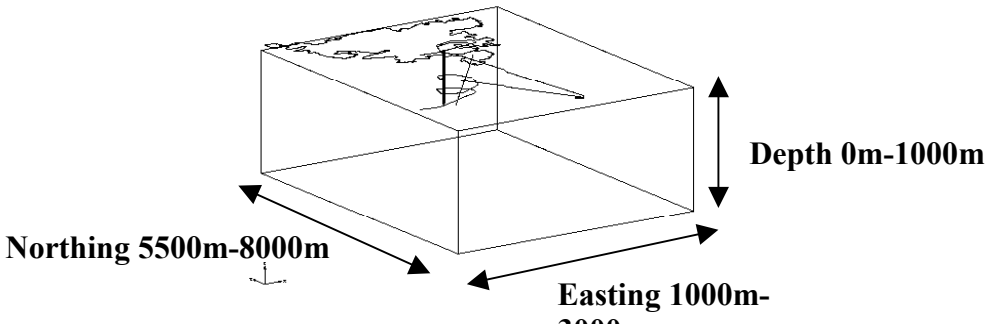

(1) Modeling area

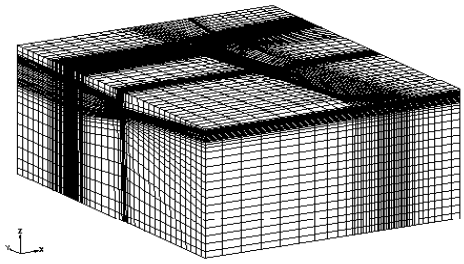

(2) Hexahedral element

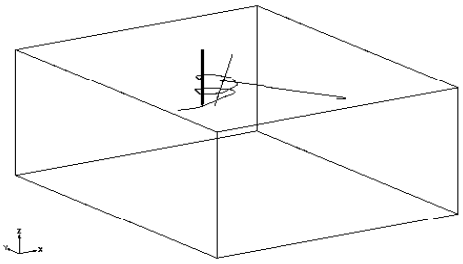

(3)Line element

Figure 6. *Modelling area and finite element diagrams.*
(The modelling area consists of ***159,214*** *hexahedral elements and* ***349*** *line elements, and the HCD is modelled by the smeared fracture model.)*

4.2 Boundary conditions of groundwater flow

The unsteady state of groundwater flow and geochemical distribution during tunnel construction were simulated by considering the progress of tunnel construction. The progress was expressed by changing the hydraulic conductivity of the tunnel with time.

Excluding the grouting and skin effect, the measured inflows at the weir were assigned to the tunnel sections as the flux boundary. The inflows have been measured at tunnel sections divided by the weir. The progress of the tunnel and the flux to the tunnel section were modelled as shown in Figure 7.

The tunnel was modelled as a number of one-dimensional elements. The excavated tunnel was expressed by elements of high conductivity. The solid and dotted lines represent respectively the constructed/unconstructed parts of the tunnel. The sections that inflow was measured are modelled by the connection of line element; the weir is modelled as the disconnection of line element. The measured flux is expelled from the top of the node consisting of the tunnel section. Thus, the measured flux is collected from the tunnel section divided by the weir.

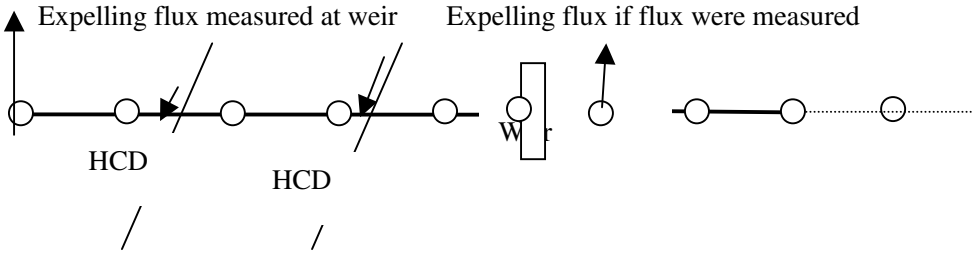

Figure 7. *The schematic illustration of flux boundary in the tunnel.*
(Arrow shows flux. Circle and line are node and line element, respectively.)

The bottom boundary and side boundary conditions were constrained as a no flux boundary and hydrostatic pressure, respectively. In the upper part of modelling area, the area of Äspö was modelled as a flux boundary and the other area of Äspö is modelled as a constant head (i.e. Baltic Sea level). The infiltration rate applied to the Äspö area is determined by representing the pressure distribution under Äspö measured before tunnel construction. The measured excess hydraulic pressure is around 5 m at level –50m under Äspö (Rhen, 1997, pp.201). The relationship between the hydraulic conductivity of the rock mass and infiltration rate is shown in Table 2. These infiltration rates create around 5 m excess pressure at level –50m under Äspö. It is assumed the infiltration rate is constant during tunnel construction.

Table 2: The relationship between the hydraulic conductivity of the rock mass and infiltration rate

Hydraulic conductivity of HRD	Isotropy (1.5×10^{-9} m/s)	Isotropy (6.0×10^{-9} m/s)
Infiltration rate	2.6 mm/year	11.0 mm/year

4.3 Initial and boundary conditions of geochemical distribution

The initial and boundary conditions are given by interpolation from the results of the M3 calculations (Gurban et al., 1998.) The changes of boundary conditions with time were neglected in this study. The boundary of the tunnel is constrained as a no concentration gradient.

4.4 Simulated conditions

The numerical analyses were performed using a 15-days time step. The streamline up-winding method for solute transport was used to stabilise the numerical conditions.

4.5 Data used

4.5.1 Hydraulic conductivity

The hydraulic conductivity of the Äspö bedrock is categorised into HCDs and HRDs. There are 17 HCDs around Äspö as defined and shown in Figure 8; the hydraulic conductivity of the HCD is described later. These HCDs are modelled by the smeared fracture model as mentioned before. Some HCDs (according to Rhén et al., 1997; pp.A2:14) have more than 10 m in thickness. The HCDs are expressed by the series of planes that are parallel and located at every 10 m. For example, a 30 m thickness of a HCD is expressed by three planes and the central plane is located corresponding to the geometry of the HCD. The hydraulic conductivity of the HRD is in the order of 10^{-9} m/s. The results of the hydraulic conductivity test depended on the test scale of the section selected. The hydraulic conductivity at the 3 m and 15 m scale was 1.5×10^{-9} and 6.0×10^{-9} m/s, respectively. The applied hydraulic conductivity to the HCDs and HRDs is described in Table 3.

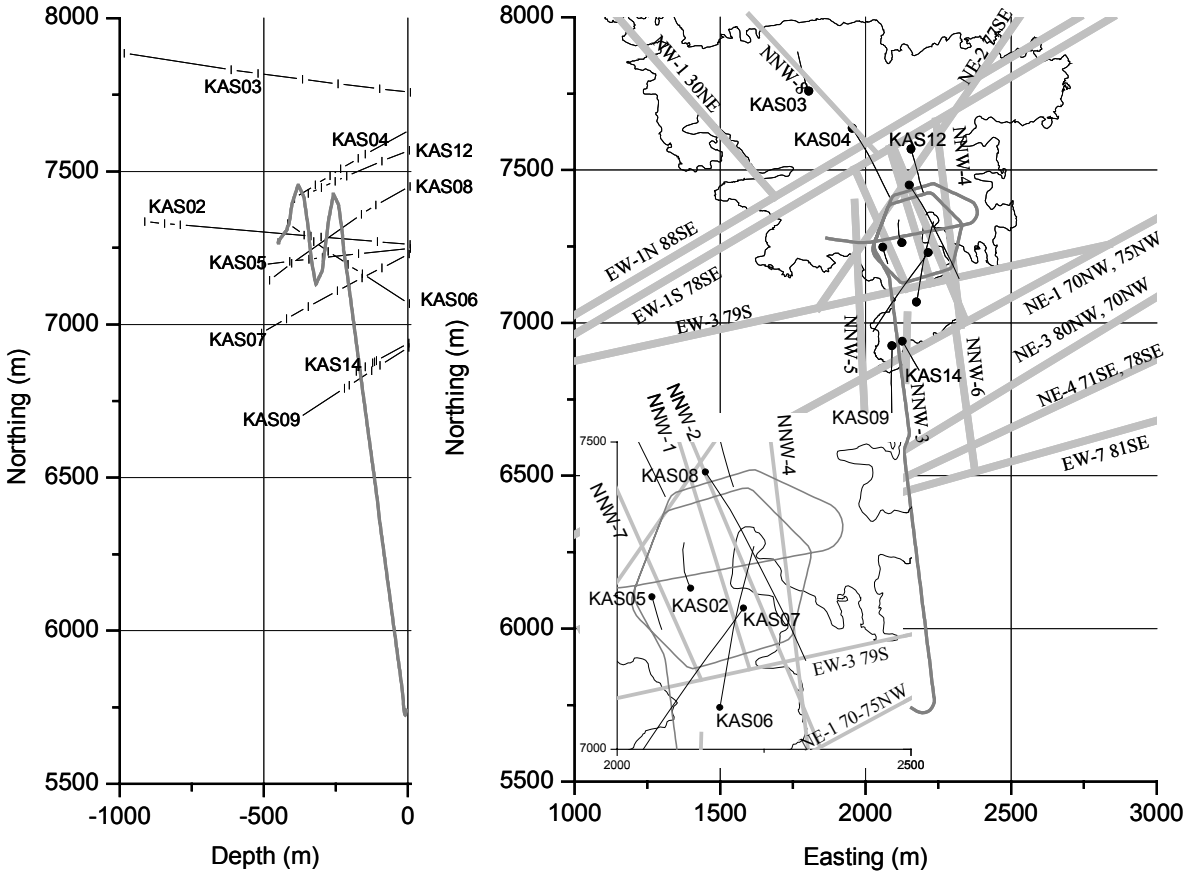

Figure 8. *Hydraulic Conductor Domains (HCDs) around Äspö based on the KAS borehole series. The map shows the intersection of the HCDs with the ground surface.*

Table 3. Hydraulic conductivity of the Hydraulic Conductor Domains (HCDs) modelled in Task 5 (Absence of values means no difference between T (initial) and T (Calibrated). "Rock mass": unit is m/sec).

Fracture Zone unit	Width m	T(Initial) m^2/sec	T(Calibrated) m^2/sec	Comments
EW-1N_r	30	5,20E-07		
EW-1S_r	30	1,20E-05		
EW-3$_r$	15	1,70E-05		-300<z<0 Upperside
lower side	15	5,00E-07		z<-300 ower side
EW-7$_r$	10	1,50E-05		
NE-1$_r$	30	2,20E-04		S=2.6e-5,ne=7.0e-3
NE-2$_r$	5	1,20E-07		
NE-3$_r$	50	3,20E-04		
NE-4$_r$	40	3,10E-05		NE-4s+Ne-4n
NW-1$_{wp}$	10	4,10E-07		
NNW-1$_{wp}$	10	8,60E-06		S=5.0e-6
NNW-2$_{wr}$	20	2,40E-05		S=2.0e-6,ne=3.4e-3
NNW-3$_{wp}$	20	2,00E-05		
NNW-4$_{wr}$	20	6,50E-05		
NNW-5$_{wp}$	10	4,00E-06		
NNW-6$_{wp}$	20	1,40E-05		
NNW-7$_{wé}$ Ä	20	7,50E-06	1,50E-05	
NNW-8$_{wé}$ Ä	20	8,40E-06		
Rock Mass	1	1,50E-09	6,00E-09	

4.5.2 Specific storage

The compressibility of granite is very small. On the basis of the definition of specific storage as given in Eq. (7),

$$S_s = \rho g(n\beta + \alpha_o) \quad (7)$$

Where ρ: water density, g: gravity, n: porosity, α_o: the compressibility of rock mass, β: the water compressibility.

The specific storage is estimated to be in the order of 10^{-6} (1/m). Rhen et al. (1997, pp.215) derived the relationship between the hydraulic conductivity and specific storage from the interference test performed at Äspö. However, this relationship gives very small values if the hydraulic conductivity is small. Thus, a specific storage value of $1.0x10^{-6}$1/m was used both for the HCDs and the HRDs.

4.5.3 Effective flow porosity

At Äspö the effective flow porosity was obtained from some tracer tests. Rhén et al. (1997, pp.399) derived the relationship between hydraulic conductivity and effective porosity as given in Eq. (8):

$$n_e=34.87K^{0.753} \quad (8)$$

Where K is the hydraulic conductivity in m/sec.

This relationship was used for assigning the effective flow porosity.

4.5.4 Dispersion

In general, the dispersion length depends on the scale of tracer movement. The longitudinal dispersion is generally assumed to be one tenth of the movement scale and the transverse dispersion will be one tenth of the longitudinal dispersion length. Around Äspö several scales of tracer tests have been performed that show the scale dependence. In this simulation 100 m is used as the longitudinal dispersion length and 20 m was used as the transverse dispersion taking into account the scale and numerical stability of calculation.

5. Simulated results and discussion

The groundwater flow and transport of geochemical components during tunnel construction were simulated. The process of the simulation is shown in Figure 9.

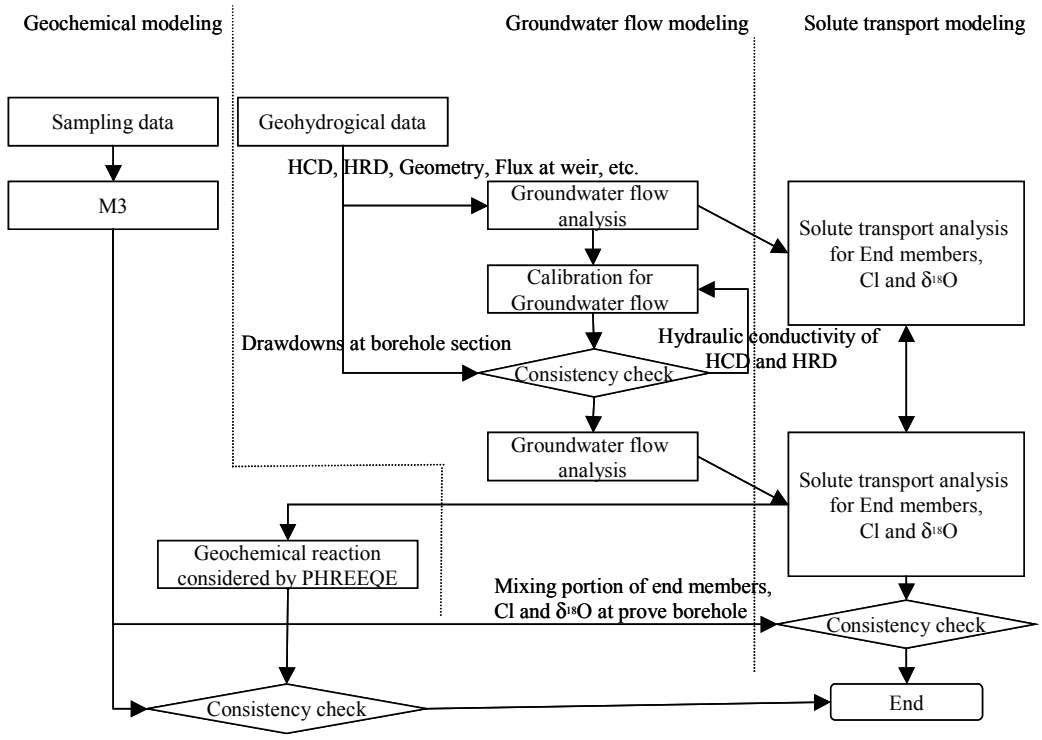

Figure 9. *Schematic flow chart of modelling work.*

5.1 Groundwater flow

5.1.1 The features of measured drawdowns

The remarkable changes in drawdowns were measured between Oct. 1992 and Oct. 1994.at the selected monitoring points, i.e. KAS02-09, KAS12 and KAS14. The high drawdowns in Oct. 1992 were caused by shaft construction. The construction of the spiral tunnel led to the drawdowns increasing between Oct. 1992 and Oct. 1994.

To understand the drawdown influenced by tunnel and shaft construction, the relative position between the HCDs, tunnel and shaft and inflow rate supplied from the HCDs should be identified. Focusing on the relative position, shaft cross NNW-7 and spiral tunnel cross NNW-1, NNW-2, NNW-4, NNW-7 and NE-2, are shown in Table 4.

Focusing on the flux, high inflow rates of more than 100 litres/min were observed at Shaf220, MA3179G and MA1584G located under Äspö. These tunnel sections cross NNW-7, NNW-4 and EW-3. In addition, the relatively high inflows of more than 100 litres/min were observed crossing certain HCDs, e.g. MA2178G, MA2994G and MA3179G crossing NNW-4, Shaft220, MA2357G, MA2699G and MA3411G crossing NNW-7. In particular, high inflows were expected to cross NNW-4 or NNW-7.

The measured fluxes related to NNW-4 and NNW-7 are shown in Figures 10 and 11. On the flux from NNW-4, no correlation was seen in spite of high flux supplied through NNW-4. Since the transmissivity of NNW-4 is high, there is no interference for each flux as shown in Figure 10. Otherwise, the total flux from NNW-7 is nearly constant and therefore high drawdowns are expected.

Since high drawdowns were expected at the monitoring sections crossing the HCDs, the relationship between borehole and the HCDs is summarised in Table 5. High drawdowns were observed at some sections crossing NNW-1, NNW-2, NNW-7 and NE-2. However, they were observed not only in the monitoring sections crossing the HCDs but also in the other sections, e.g. the upper section of KAS02 and KAS05. Since these sections are close to the position of the shaft, such high drawdowns are possible. From this relationship, it is important to identify the geometric information between the tunnel and monitoring section as well as that between the HCDs and monitoring sections.

NNW-4 and NNW-7 are important to evaluate the flux of groundwater. The HCDs crossing the spiral tunnel, e.g. NNW-1, NNW-2, NNW-4, NNW-7 and NE-2, are important to evaluate the drawdown. To predict the drawdown, the relationships between the progress of tunnel construction, the HCDs and monitoring sections are important.

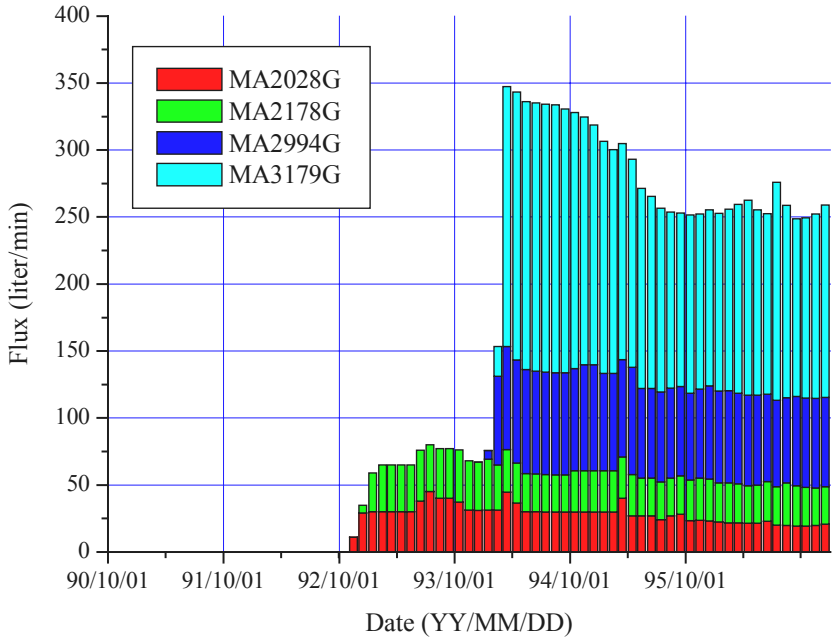

Figure 10. *Flux at weirs related to NNW-4.*

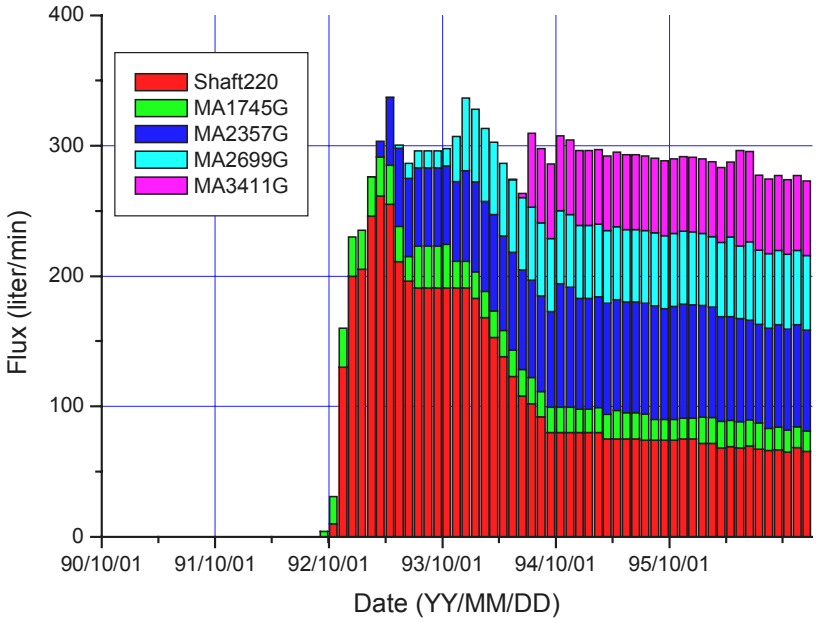

Figure 11. *Flux at weirs related to NNW-7.*

5.1.2 Calibration

The first calculation of groundwater flow was performed using the measured values of the hydraulic properties. The hydraulic conductivity of the HCDs and HRDs are given in Table 3 and the specific storage is defined as 1.0 x 10^{-6} (1/m). The simulated drawdowns for these parameters are shown in Figure 12, together with the measured drawdowns. The dots and lines show the measured and simulated drawdowns, respectively. The simulated drawdowns at some sections of KAS02 and KAS05 were much higher than the measured values. Therefore the calibration was conducted by changing the hydraulic conductivity of the HCDs and HRDs. To understand the sensitivity of hydraulic conductivity, twice the value of hydraulic conductivity was used. The case name indicates the change in the hydraulic conductivity of the HCD. For the HRD, the hydraulic conductivity was measured using the 15 m -scale (6.0 x 10^{-9} m/s) instead of the 5 m -scale (1.5 x 10^{-9} m/s). The calculated drawdowns in borehole sections of KAS02-09, KAS12 and KAS14 were compared with the measured drawdowns between Oct. 1990 and Feb. 1994. These results were summarised by using the object function as shown in Eq (9):

$$f_{obj} = \sum_{i=1}^{n} \left| h_{mea} - h_{cal} \right| \qquad (9)$$

Where: h_{mea} is the measured head, h_{cal} is the calculated head, and n is the sum total of the control points for drawdown.

The sensitivity of the change in hydraulic conductivity of the HCDs and HRDs is shown in Figure 13. The results show that the changes of hydraulic conductivity of the rock mass and NNW-7 decreased the value of the object function significantly. However, the hydraulic conductivity of the other HCDs is not so sensitive.

Moreover, through trial and error, many combinations of fracture transmissivity were tried in order to decrease the object function, but little improvement was seen. The results are shown in Figure 14. Case 1 indicates the calculated result using the calibrated value listed in Table 3. In case 1 the hydraulic conductivity of the HRDs and NNW-7 were changed from the initial value. The changes of these parameters make the object function decrease by 25% from the initial parameter setting. Thus, the calibrated value was used for subsequent calculation.

Excluding modelling the grouting and skin effect around the tunnel, numerical simulation of the groundwater flow was performed in order to model the inflow to the tunnel. The inflows observed at the weirs are shown in Figure 15; the locations of weirs are shown in Figure 16. Since the inflow flux at the weir is expected to be supplied from the HCDs, it is important to identify the relationship between the HCDs and the tunnel section divided by the weir that is used for monitoring the inflow to the tunnel. The intersections of the tunnel and the HCDs are summarized in Table 4; the intersections of the monitoring section and the HCDs are shown in Table 5. These relationships are derived from the intersections of the line elements (tunnel and borehole) and the plane equations.

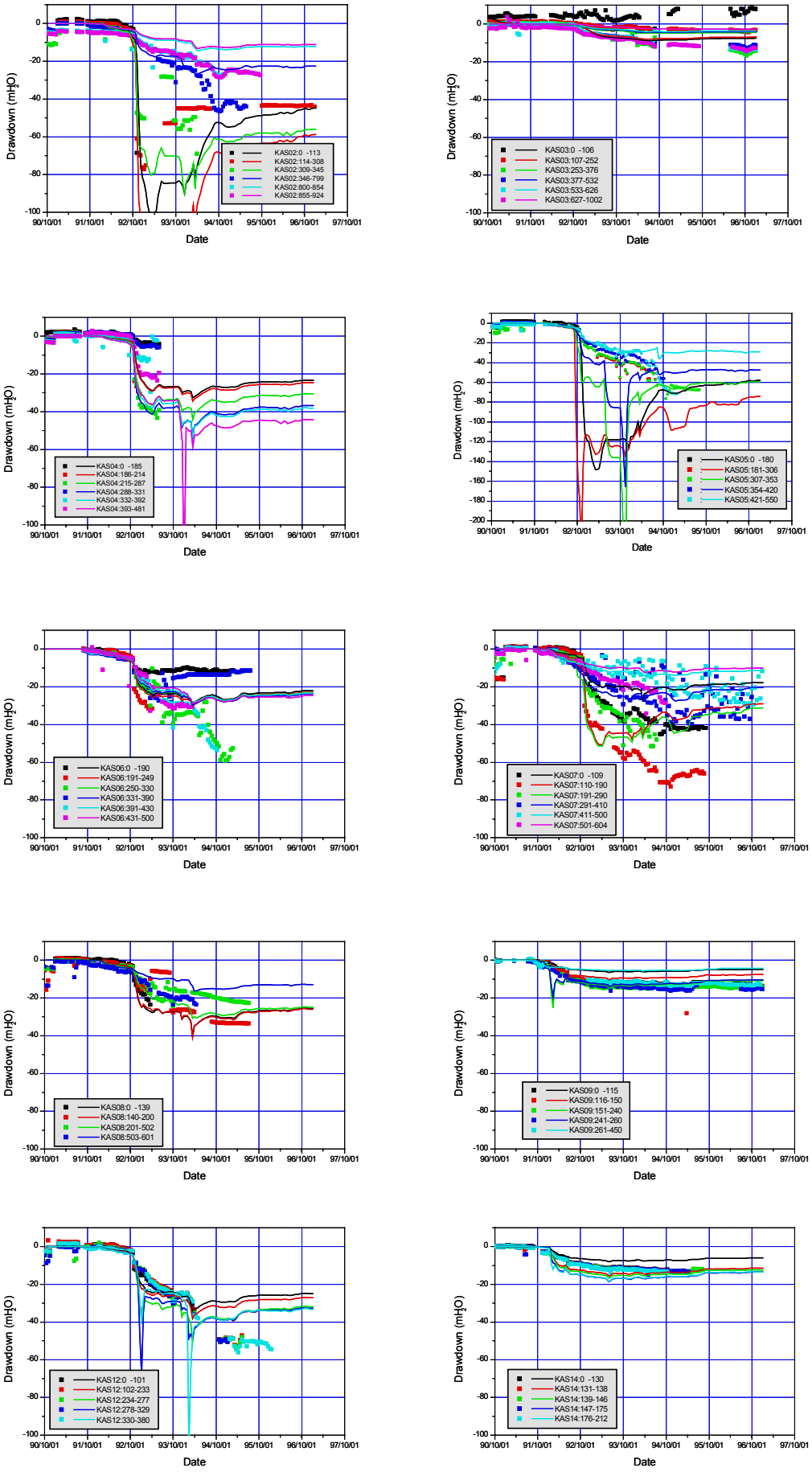

Figure 12. *Correlation between calculated and measured drawdowns at borehole sections based on initial parameter settings.*

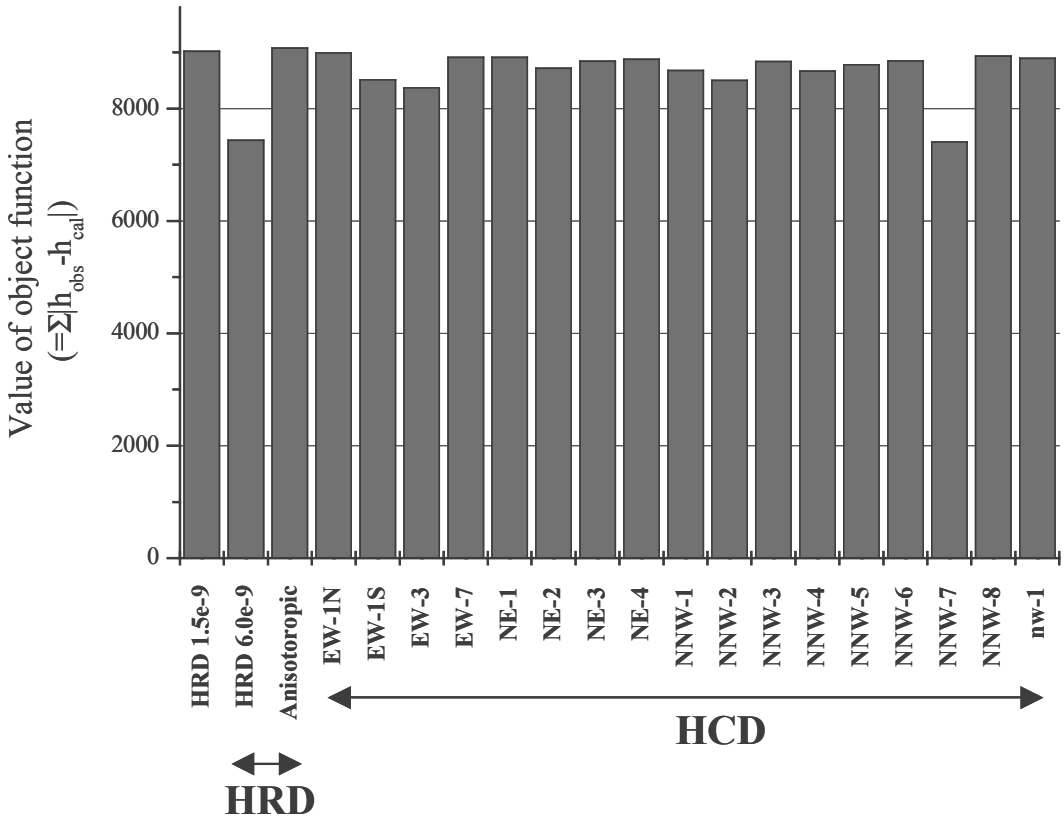

Figure 13. *Sensitivity of hydraulic conductivity for the HCDs and HRDs (The hydraulic conductivity is considered as two times of original value).*

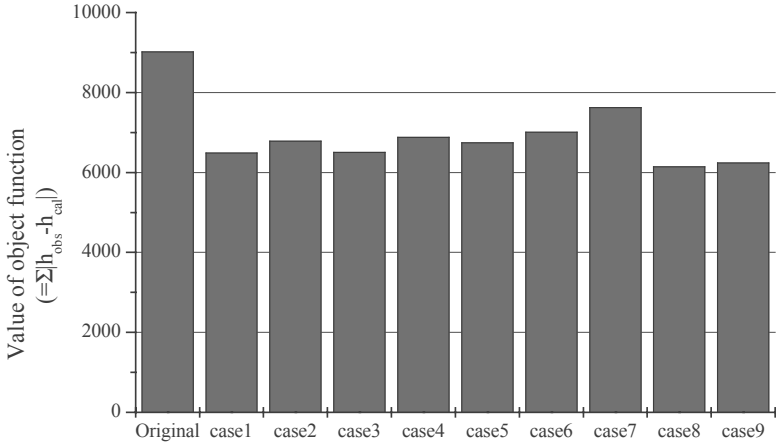

Figure 14. *The results of the trial and error method (Some kind of combination is tested to decrease the object function).*

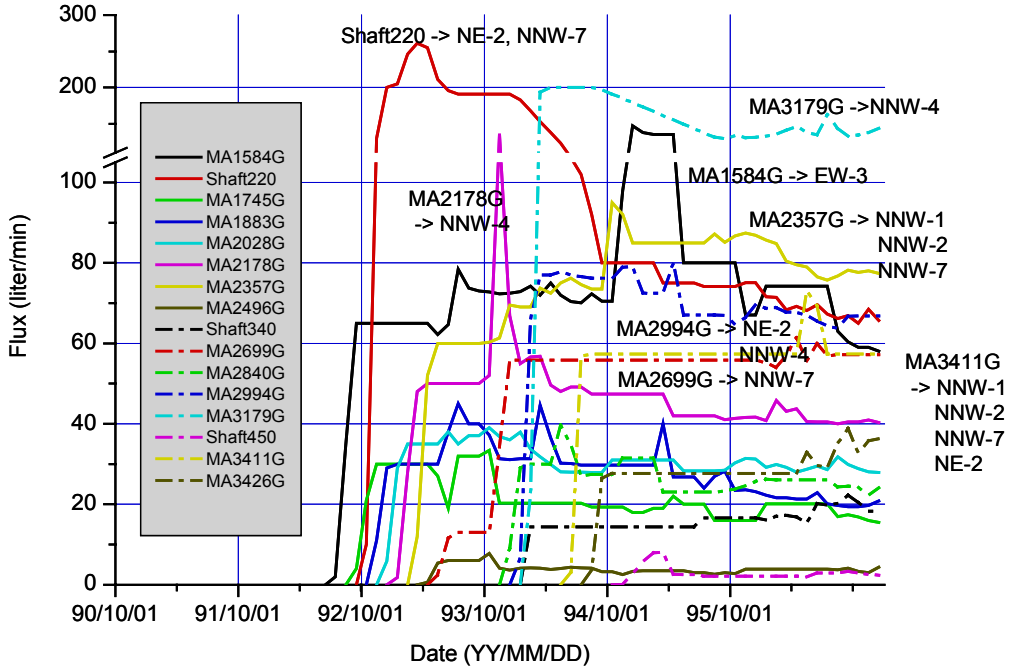

Figure 15. *Flux measurements at the weirs*

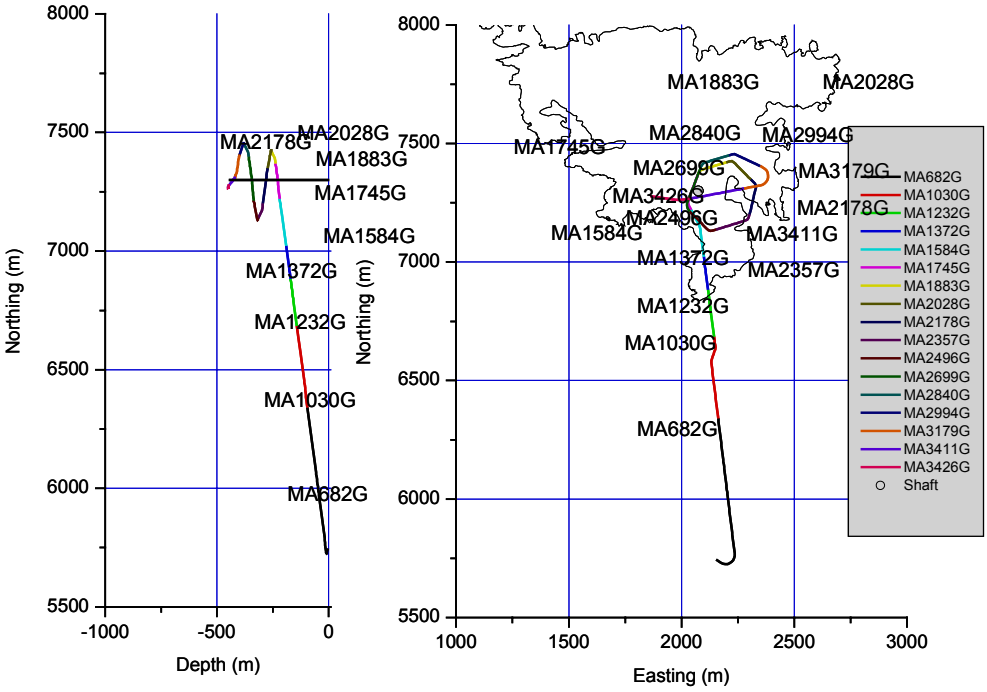

Figure 16. *Location of weirs*

Table 4. Intersection of HCDs by the tunnel sections, each represented by one weir measurement (i.e. MA686G).

HCD	MA 682G	MA 1030G	MA 1232G	MA 1372G	MA 1584G	Shaft 220	MA 1659G	MA 1745G	MA 1883G	MA 2028G	MA 2178G	MA 2357G	MA 2496G	Shaft 340	MA 2587G	MA 2699G	MA 2840G	MA 2994G	MA 3179G	Shaft 450	MA 3384G	MA 3411G	MA 3426G	MF 0061G
EW-1N																								
EW-1S																								
EW-3					x																			
EW-7		x																						
NE-1				x																				
NE-2								x	x				x	x				x				x		
NE-3		x																						
NE-4N		x																						
NE-4S		x																						
NW-1																								
NNW-1									x			x					x					x		
NNW-2									x			x					x					x		
NNW-3			x																					
NNW-4										x	x							x	x					
NNW-5																							x	
NNW-6																								
NNW-7						x		x				x				x						x		
NNW-8																								

Table 5. Intersection of monitoring sections and the HCDs.

HCD	Intersected sections by HCD			
EW-1N	KAS04:0-185			
EW-1S	KAS04:332-392			
EW-3	KAS06:0-190			
EW-7				
NE-1	KAS07:501-604	KAS08:503-601	KAS09:0-115	KAS14:0-130
NE-2	KAS02:346-799	KAS05:421-550	KAS12:330-380	
NE-3	KAS09:261-450			
NE-4N				
NE-4S				
NW-1	KAS03:107-252	KAS04:215-287		
NNW-1	KAS06:250-330	KAS07:0-109		
NNW-2	KAS06:391-430	Close to KAS08		
NNW-3	KAS14:0-130	Close to KAS09		
NNW-4				
NNW-5	Close to KAS09			
NNW-6				
NNW-7	KAS02:346-799	KAS07:191-290	Close to KAS02 and KAS05	
NNW-8	KAS03:377-532			

5.1.3 The simulated drawdowns

The simulated drawdowns using calibrated parameter listed in Table 3 are shown in Figure 17. The drawdown trends were roughly represented.

.

The major refinements and their effect on the simulated results are as follows,

- The drawdowns near the shaft, i.e. the upper sections of KAS02 and KAS05:0-180, were improved by changing the hydraulic conductivity of NNW-7. Since the inflow was modelled as a flux boundary, the drawdown of the shaft crossing NNW-7 depended on the hydraulic conductivity of NNW-7.
- All sections of drawdowns are a little lower using the hydraulic conductivity of 15 m-scale tests, which is four times that of the 3 m-scale ones. This indicates that the hydraulic conductivity of the HRDs is also important to evaluate the drawdown.
- The drawdowns at some sections of KAS05 were improved by refining the relationship between the location of weirs and the HCDs shown in Table 4. These mismatches were caused by coarse discrimination of finite elements.

The main inconsistencies are as follows,

- The simulated drawdowns are a little lower than those measured at some sections of KAS12 close to NE-2, and KAS06:250-330, KAS06:390-430 and KAS07:0-109 crossing NNW-1 and NNW-2. At these HCDs, i.e. NNW-1, NNW-2 and NE-2, there is relatively low hydraulic conductivity and not so much flux is supplied to the tunnel. They are important to simulate drawdown at the monitoring sections. For them, a lower hydraulic conductivity more accurately represents the measured drawdown.
- The simulated drawdown at KAS05:181-306 is higher than that measured. Here the inflow is assigned to the tunnel section and the drawdown occurs along the tunnel as well as at the intersection of the tunnel with the HCDs. There is a possibility that the calculated drawdown at the upper section of KAS02 and KAS05 is influenced by the drawdown at the tunnel. Since this section is close to NNW-7 and the mesh is not so fine, it reflects the drawdown within NNW-7. In both cases, since this inconsistency is caused by modelling methods, it is difficult to refine.
- The main features of drawdown were roughly represented by the simulations. However, the drawdown at KAS07:110-190 could not be represented and explained by the relationship between the tunnel and the HCDs.

These drawdown simulations demonstrate that it is quite important to simulate the event, such as shaft and tunnel construction, to represent the measured drawdown. These temporal and geometric relationships provide the information, i.e. the cross-section of tunnel and the HCDs, the inflow via the HCDs, and the drawdown via the HCDs. These are quite important to identify which HCD causes the drawdown. In particular, the drawdown timing indicates which HCD is important to evaluate the drawdown. Therefore, an unsteady state of groundwater flow gives much information to refine the hydrogeological model.

In conclusion, the modelling exercise shows that the timing and amount of measured drawdowns are roughly represented by the simulations, thus providing confidence in the properties and geometry of the hydrodynamic model.

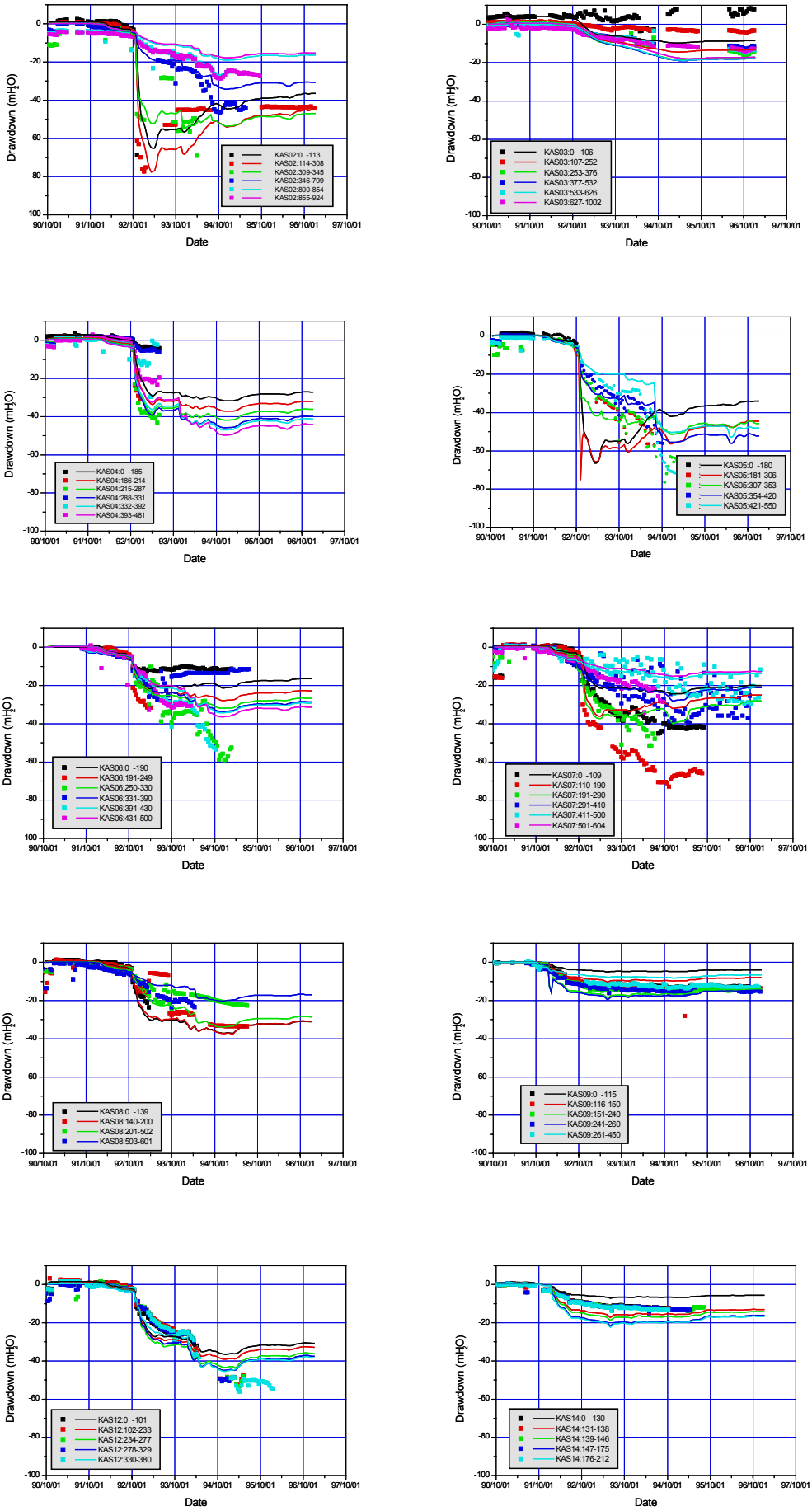

Figure 17. *Correlation between calculated and measured drawdowns at borehole sections based on calibrated parameter settings.*

5.2 Geochemical conditions

5.2.1 Changes in geochemical distribution

As mentioned in section 2.3, in the shallow groundwaters, the mixing proportions of Meteoric and Baltic sea water were high at the initial conditions, e.g. at KR0012B, SA0813B and SA1229A. On the other hand, in the deep groundwaters, those of Glacial and Äspö Brine water were high at the initial condition, e.g. SA2074A, SA2783A, SA3005A, KA3110A and KA3385A.

The mixing portions of Meteoric and Baltic water increased with the progress of the tunnel construction. According to the calculation results of M3, the initial groundwater composition was mainly replaced by meteoric water, except for KA2783A. At the monitoring point of KA2783A, the mixing portions of Glacial and Äspö Brine water were increasing.

Since the Cl concentration depends on the depth, the initial concentration is low in the shallow part and high in the deep part at the initial conditions. The value of $\delta^{18}O$ is high in the shallow part and high in the deep part at the initial conditions. But meteoric water infiltrated from Äspö is low in Cl with a lower $\delta^{18}O$ value. Since the properties of meteoric water are different from the distribution trend, it needs attention to evaluate the groundwater flow during tunnel construction.

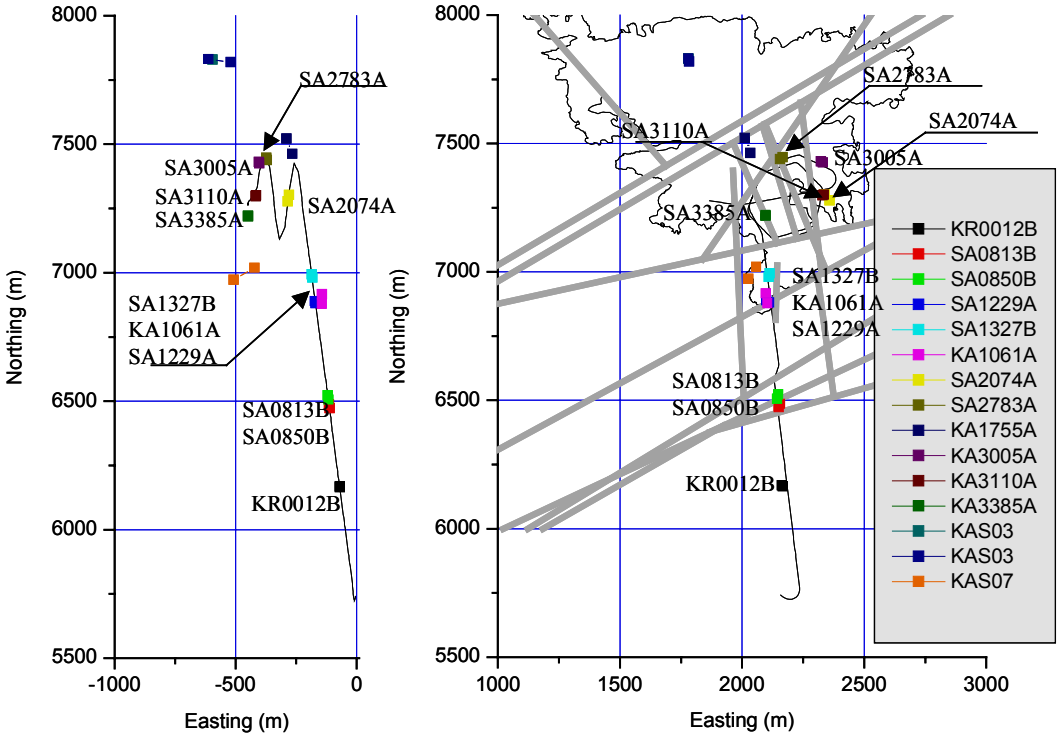

***Figure 18**. Location of monitoring points for geochemical evaluation.*

5.2.2 Expected groundwater flow to control point

From the geometric point of view, these control points were categorised into several groups. KR0012B, SA0813B and SA1229A are located within the straight part of the tunnel prior to its entrance under Äspö; the others are located along the spiral part around the HCDs. SA2074, KA3005A and KA3110A are close to NNW-4, and SA2783A and KA3385B are close to NNW-2 and NNW-7, respectively.

For KR0012B, SA0813B and SA1229A, the groundwater simply flows from the top boundary to the tunnel and not much mixing from the bottom boundary is expected since the monitoring points are close to the upper boundary.

At the monitoring points related to NNW-4, e.g. SA2074, KA3005A and KA3110A, the higher groundwater flow via NNW-4 is measured and, as expected, the flux comes from the Baltic Sea. The mixing proportions of these monitoring points are therefore going to be close to Baltic Sea water.

For SA2783A and KA3385B, since these HCDs are intersected by the tunnel many times, the flux from NNW-2 and NNW-7 is relatively small and some water collected from the deeper part is expected.

5.2.3 The simulated geochemical distribution

The simulated geochemical distributions at the monitoring points are shown in Figures 19 and 20. Figure 19 shows the mixing proportions of the four-end members at the monitoring points; Figure 20 shows the conservative tracers at the monitoring points.

For KR0012B, SA0813B and SA1229A the groundwater simply flows from the top boundary to the tunnel as expected, and this results in the groundwater being replaced by Baltic Sea water and Meteoric water. Since the groundwater flow occurred when the tunnel passed the control points, the groundwater flow is caused by the tunnel construction. However the simulated mixing portions of Baltic and Meteoric did not closely agree with the M3 results.

Sections SA2074, KA3005A and KA3110A cross NNW-4 that supplies the high inflow to the tunnel. SA2074 is located at the first circle of the spiral tunnel and shows that the groundwater was replaced by Baltic Sea water and Meteoric water. The change in mixing proportions was caused by the groundwater flow path change due to tunnel construction as shown in Figure 21. The groundwater of KA3005A and KA3110A is influenced by the intrusion of Baltic Sea water via NNW-4. However, the M3 results show the groundwater to be replaced by Meteoric water rather than Baltic Sea water.

For SA2783A, the remarkable intrusion of Baltic Sea water was seen followed by an increase in the rate of Glacial water and Äspö Brine water associated with the progress of tunnel construction. According to the M3 calculations groundwater could move from deeper to shallow depths. For KA3385B, the groundwater movement mostly represents the intrusion of Meteoric water, but also some from greater depths. The simulation results are in good agreement with the M3 calculations.

With regard to the simulation results of mixing proportions and flow direction, since the groundwater velocity is quite high, the changes in mixing proportions were derived by the change of flow path after the tunnel was excavated. Hence these changes are caused by the boundary conditions in the simulation.

The M3 calculations show that the deeper part of groundwater will be replaced by Meteoric water. But if it is assumed that the infiltration rate is several tens of mm/year and the area of Äspö is around 1 million m^2, the total infiltration of meteoric water at Äspö may be only a few tens of litres/min. In contrast, this estimated infiltration is much lower than the total inflow to the tunnel measured at the weirs under Äspö, i.e. around 600 litres/min. Therefore it is natural the groundwater at the deeper part is replaced by Baltic water in the simulation.

There is a possibility that this inconsistency is due to the difference between the global groundwater flow and local groundwater flow at the borehole section or the effect of storage water outside the volume of effective flow porosity. In this model, the local groundwater flow is neglected, i.e. the double porosity approach. From this point of view further study is needed to obtain better agreement with the geochemical conditions.

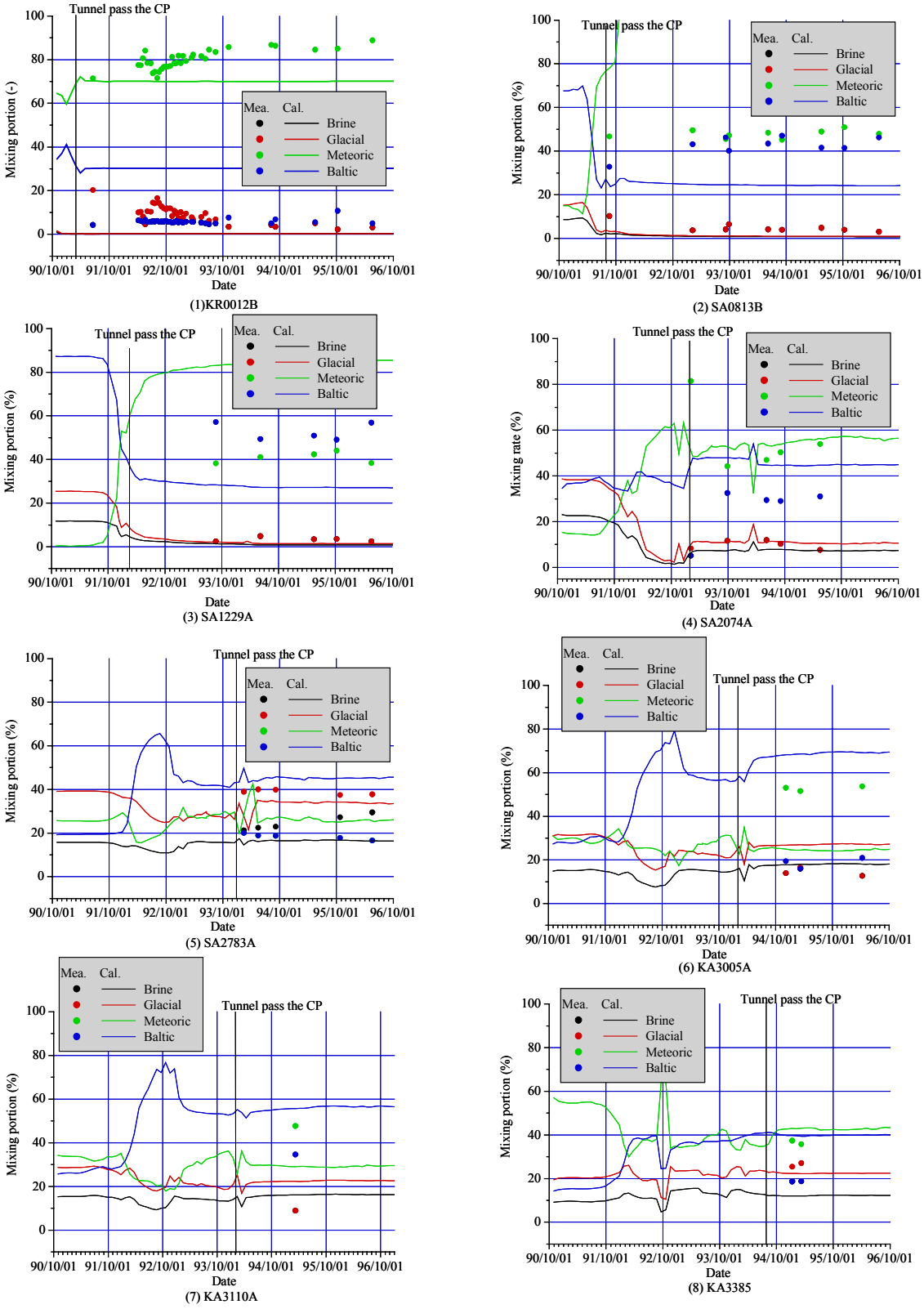

Figure 19. *Simulated mixing proportions of end members at monitoring points.*

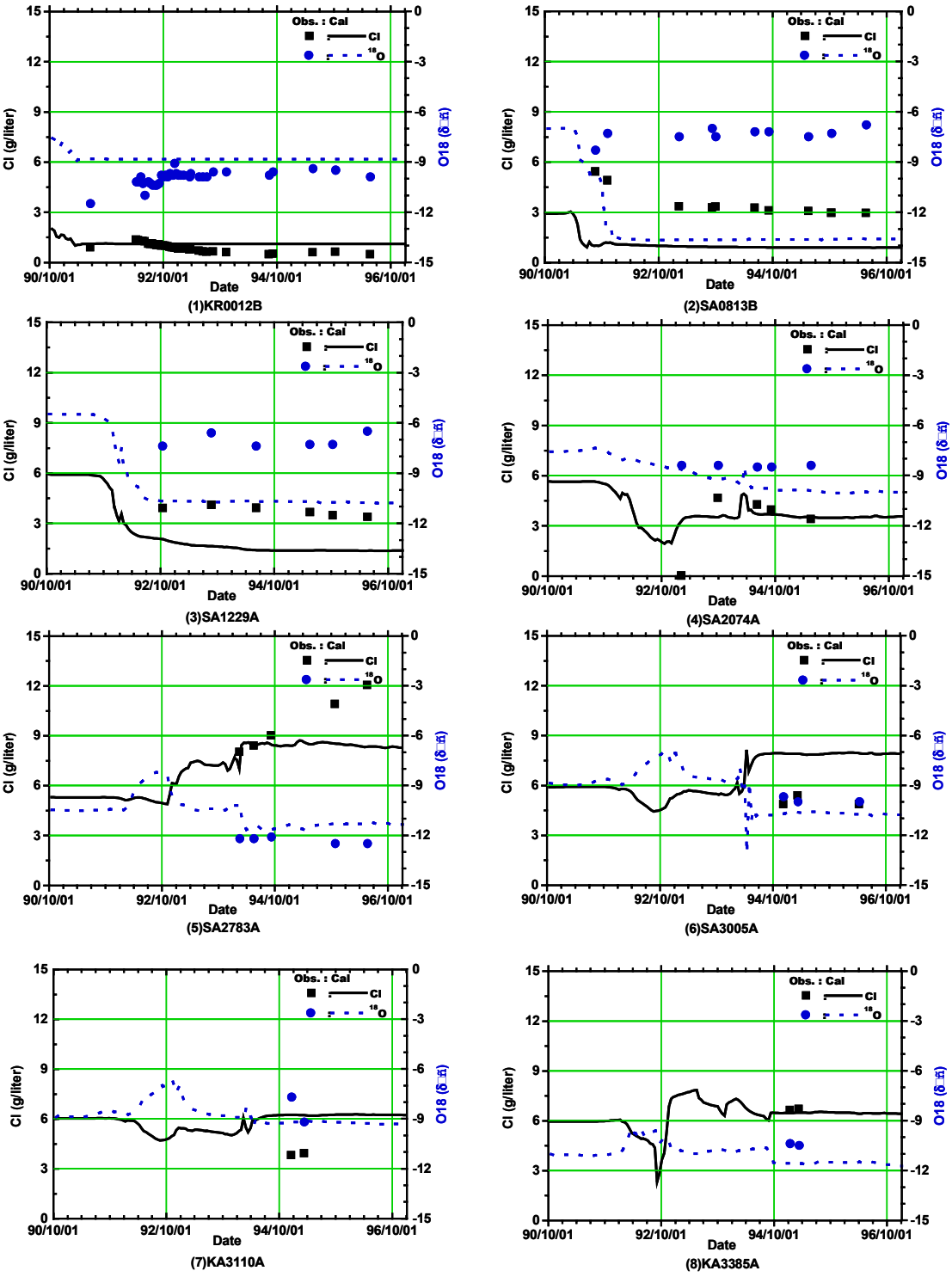

Figure 20. *Concentration changes of conservative tracers during tunnel construction.*

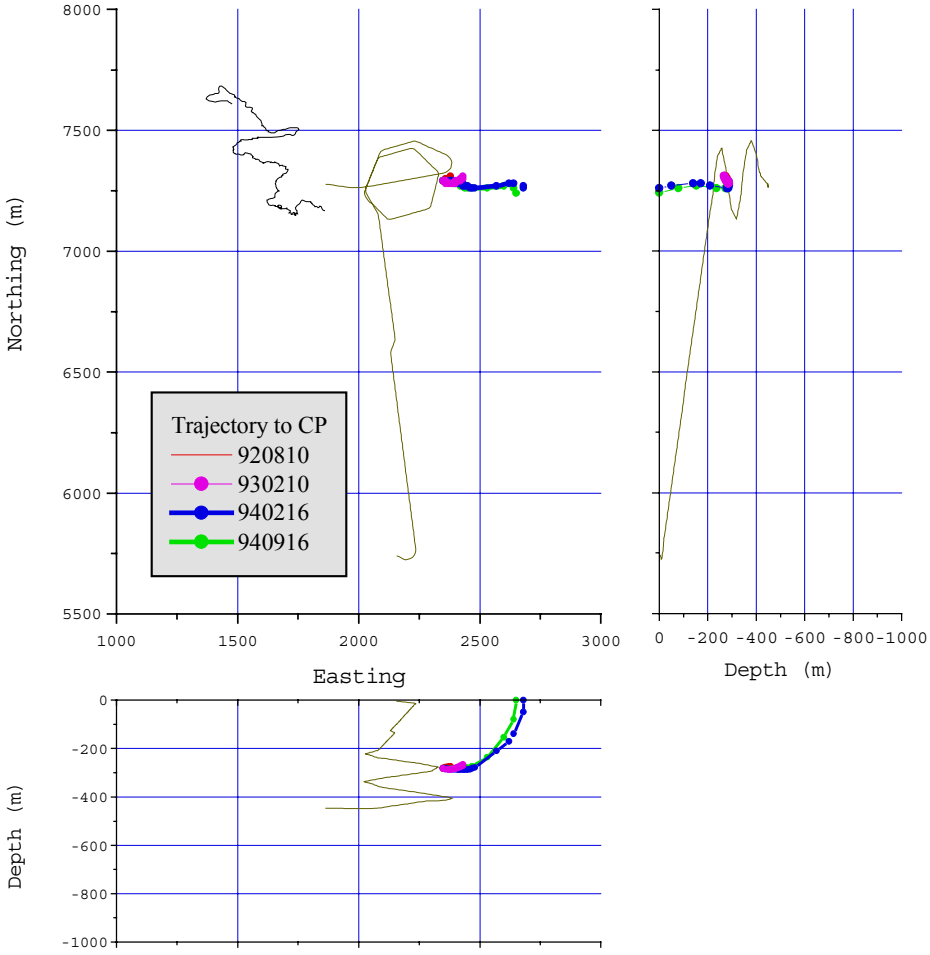

Figure 21. *Trajectory to monitoring point (SA2074). (The colours of lines show the change of trajectory with time.)*

6. Helium concentration

6.1 Background

CRIEPI has participated in several Äspö international cooperation projects since 1992. Several years ago this included the application of an independent groundwater dating method developed externally by CRIEPI. This involved the sampling of groundwaters from probe boreholes in the tunnel in 1995 and 1997; these were analysed for noble gas contents, isotopes (e.g. tritium) and major ion concentrations. Based on the helium concentrations, numerical calculations have been performed to provide additional information to help understand the groundwater flow system.

6.2 Main features of helium

In order to check the consistency between the chemical properties of the collected samples and groundwater flow modelling, numerical calculations have been performed. In particular, it is easy to simulate the dissolved He concentrations. The reasons are as follows:

- The boundary conditions are quite simple to evaluate the distribution of He. For example, the source of He is a constant rate production from the rock and therefore the concentration of He will be an atmospheric equilibrium concentration at the ground surface.
- The flow field can be simply determined. For example, since the He concentration depends on the residence time, the He concentration will be lower with shorter residence times and will be higher with longer residence times.

6.3 Model description

Since the geological model used corresponds to that mentioned in Chapter 4, only additional conditions are described in this section. The boundary conditions on groundwater flow and He transport are those shown in Figure 22. The production rate value from the rock was estimated from the contents of U and Th in the rocks collected from the drillcores. The flux value of He representing the bottom boundary condition was estimated from the value measured at the Great Artesian Basin in Australia by Torgersen and Clarke (1987). The parameters of He transport are summarised in Table 6.

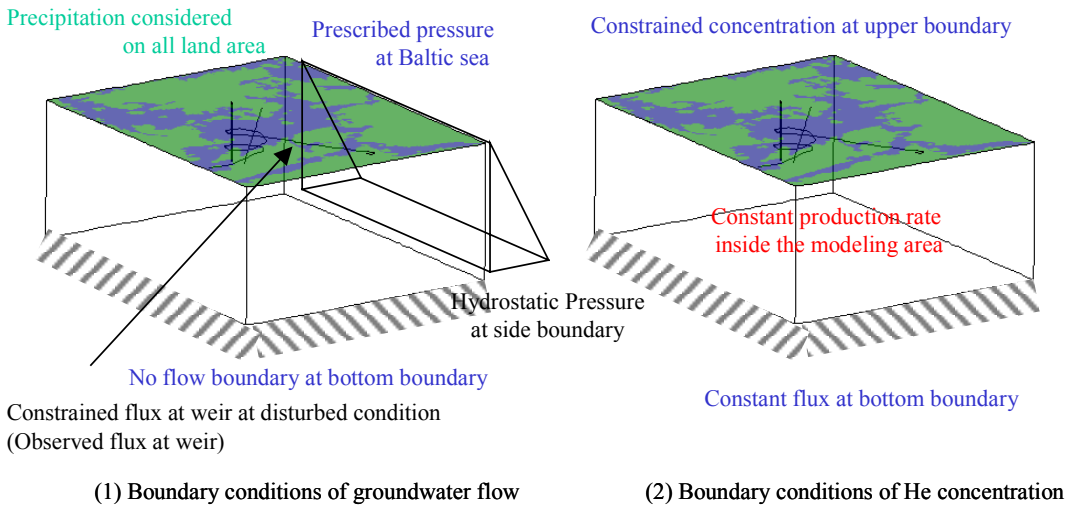

Figure 22. *Description of boundary conditions constraining He transport.*

Table 6: Parameter setting for helium transport

Parameter	Input value
Production rate	1.0×10^{-9} ccSTP/g (w)
Flux from the bottom	3.6×10^{-8} m^3/m^2year
Dispersion length	DL: 100m, DT: 20m
Diffusion coefficient	D 0.17m^2/year
Infiltration rate	2.6mm/year

6.4 Calculated results

As shown in Figure 23, since the helium concentration will be higher with longer residence times, it will therefore tend to increase with increasing depth. The concentration is divided into three categories, mixing zone, unchanged zone, and fracture flow zone. The concentration of KA2783, KA3110A, KA3385A and KA3510 are close to NNW-2, NNW-4, NNW-7 and NNW-5, respectively. The concentrations influenced by HCDs are lower than others, in particular that of KA3110A is low because of the high conductivity of NNW-4.

The undisturbed and disturbed conditions of He transport were calculated. These conditions indicate before and after tunnel construction, respectively. In the undisturbed condition it is assumed that the groundwater flow is induced by rain infiltration. In disturbed conditions the groundwater flow into tunnel was modelled as a constrained flux boundary at the tunnel. The steady state of groundwater flow and solute transport was simulated. The outline of the calculation is shown in Table 7 and the calculated results are shown in Figure 23.

The simulated concentrations in undisturbed condition agree with the measured concentration. He transport in the undisturbed and disturbed condition was simulated since the effects of meteoric water intrusion via HCDs were roughly represented.

The concentration is in atmospheric equilibrium at the upper boundary. The concentration in the modelling area depends on the dispersion rate, the infiltration rate, the production of He from the rock and the flux from the bottom boundary. In these parameters, the dispersion and the infiltration rate are sensitive, but these have many uncertainties since it is difficult to measure. In this calculation, the dispersion is roughly in proportional the infiltration rate by using the dispersion length. Therefore the infiltration rate is changed in simulation to decrease the parameter.

The simulated concentrations in disturbed conditions are much lower than those measured. It indicates that the groundwater intrusion and dispersion are much higher than before tunnel construction. But it is not clarify when the concentration reach the steady state after tunnel construction. From these results, these is a possibility that the concentration will decrease with time.

Although the simulation model of He transport consists of simple assumptions, the simulated concentrations before tunnel construction are in good agreement with measured concentrations. Since the simulated and measured concentrations reflect the properties of HCDs, it is a useful check of the hydrogeological model.

Table 7: Calculation outline for helium concentration

Case	**Outline**	
Observed	Observed value from sampling	
Calculated	Undisturbed	No precipitation
		2mm/year
		0.2mm/year
	Disturbed	2mm/year
		0.2mm/year

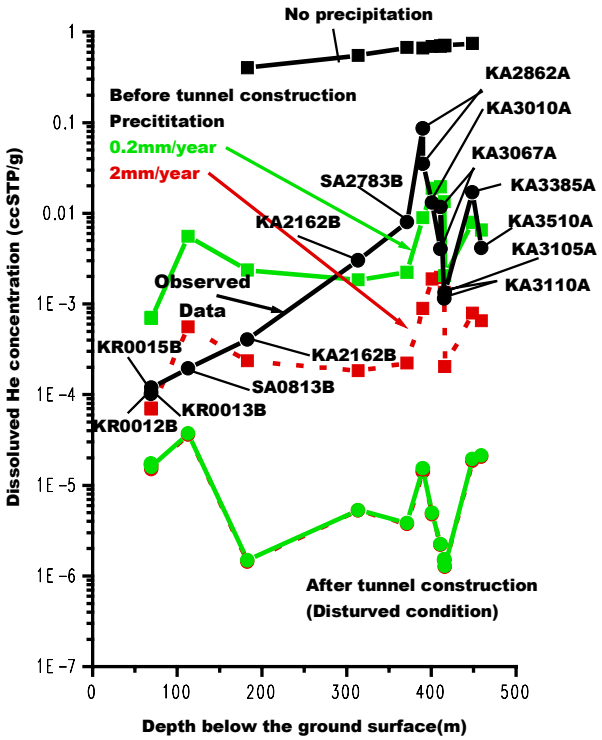

Figure 23. *Observed and calculated dissolved He concentrations.*

7. Geochemical reactions

7.1 Background

To facilitate integration of hydrochemical data with the hydrodynamic modelling exercise, a dataset of mixed groundwater proportions from each of the groundwater control points and based on four end-members (i.e. Meteoric, Baltic, Äspö Brine and Glacial water), was distributed to the Task#5 participants. The initial and boundary conditions of the mixing calculation were based on principle component analysis using the M3 approach (Multivariate Mixing and Mass balance calculations) after Laaksoharju (1999). These mixing proportions did not consider in detail the possible influence of geochemical reactions.

In this present study, the hydrodynamic simulated geochemical distributions based on the M3 mixing proportions indicated some inconsistencies (see section 5.2.3). To test whether some of these inconsistencies reflect the potential effect of geochemical reactions on the groundwater chemistry, the PHREEQE code has been used.

7.2 Modelling process

The concept of the geochemical modelling used in this study is shown in Figure 24. The modelling consists of three processes. First, the initial compositions of four end members are defined based on the measured chemical compositions (e.g. Meteoric, Baltic, Äspö Brine and Glacial water). Second, the chemical properties of the mixed water are calculated from the mixing ratio predicted by the M3 results. In this step, chemical reactions are not taken into account. Finally, several equilibrium geochemical reactions are introduced to the calculated chemical compositions at the second step to identify the reactions that evolve groundwater chemistry. The HARPHRQ (Brown et al, 1991) code is used for the calculation, together with the geochemical database, HATCHES (Cross et al., 1990), which was developed by the UKAEA. In addition, cation exchange reactions are also considered.

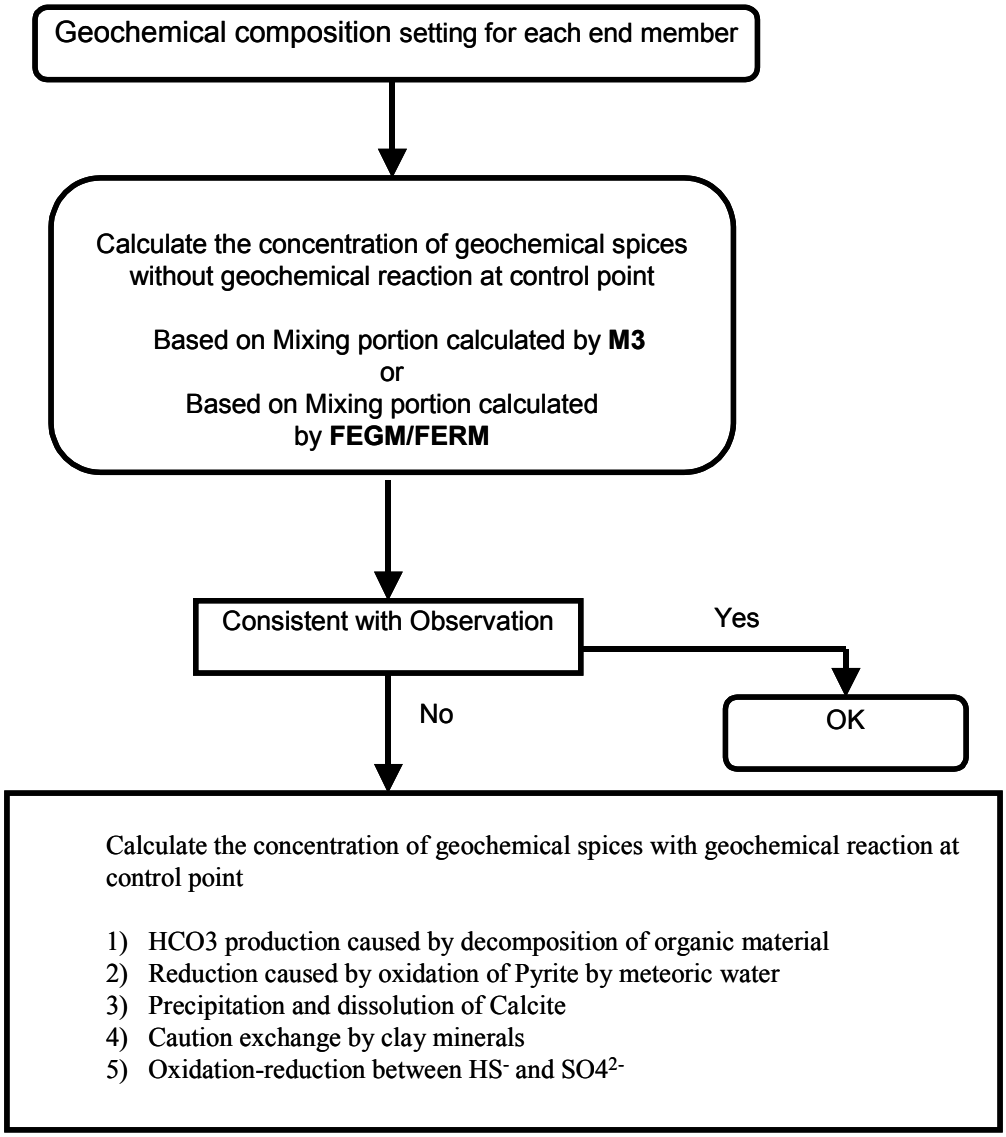

Figure 24. *The evaluation process of geochemical reactions in this study.*

7.3 Geochemical reactions considered

Based on 'Groundwater reactions to consider within the Task 5 modeling', provided as guidelines by Task 5, the following reactions were selected:

1) HCO_3 production caused by decomposition of organic material in meteoric water
2) Consumption of dissolved oxygen in meteoric water by pyrite oxidation
3) Precipitation and dissolution of calcite
4) Cation exchange by clay minerals
5) Oxidation-reduction between HS^- and SO_4^{2-}

7.4 Assumptions

The chemical compositions of the four end members are shown in Table 8 and the observed chemical compositions of groundwater samples at the evaluation control points are shown in Table 9.

Table 8: Representative chemical compositions of the four end members

Reference Water	Na	K	Ca	Mg	HCO_3	Cl	SO_4	D	Tr	^{18}O
Äspö Brine	8500	45.5	19300	2.12	14.1	47200	906	-44.9	4.2	-8.9
Baltic Sea	1960	95	93.7	234	90	3760	325	-53.3	42	-5.9
Glacial	0.17	0.4	0.18	0.1	0.12	0.5	0.5	-158	0	-21
Meteoric	0.4	0.29	0.24	0.1	12.2	0.23	1.4	-80	100	-10.5

D (Deuterium) = ‰ dev SMOW; Tr (Tritium) = TU (Tritium units), ^{18}O = ‰ dev SMOW; Others = (mg/litre)

Table 9: Observed chemical conditions at the evaluated control points

ID code	Date	Brine	Glacial	Meteoric	Baltic Sea	Na	K	Ca	Mg	HCO_3	Cl	SO_4
KR0012B	960521	3.1%	3.1%	88.8%	4.9%	326.9	3.7	83.6	14.4	302	495.6	102
SA0813B	960521	3.0%	3.0%	47.8%	46.2%	1523	19.4	276	112	319	2964	252
SA1229A	960521	2.4%	2.4%	38.3%	56.8%	1640	28.0	413	137	303	3393	248
SA2074A	950518	7.6%	7.6%	53.9%	31.0%	1454	9.3	560	119	128	3414	262
SA2783A	960520	29.4%	37.7%	16.5%	16.5%	3053	10.9	4062	49	15	12054	616

Initial chemical conditions of the four end members were assumed as follows:

1) The observed pH values at almost all of the monitoring points were within the range of 6 to 9.
2) Considering the origin of the end members, the meteoric water is oxic and the others are anoxic.
3) The solubility of the calcium ion is restricted by the solubility product of calcite for brine and Baltic Sea water because of the high salinity of the two end members. The principal chemical forms of carbon and sulfur are HCO_3^- and SO_4^{2-}, respectively. Appropriate pH and pe values are selected so that the chemical compositions of the end members could meet the initial conditions.
4) The evaluated pH and pe values are listed in Table 10. The values for glacial and meteoric waters are cited from the JNC Report (1999).

Table 10: pH and pe for each end member

Date	Äspö Brine	Glacial	Meteoric	Baltic Sea
pH	6.9	7.9	8.5	8.5
pe	-3.6	-4.4	-4.75	7.98

7.5 Geochemical reaction analysis

The following reactions are considered in this study, and the structure of the geochemical modelling is presented in Figure 25.

(a) Mixing of different end members
The chemical compositions are evaluated by the mixing of different end members. No chemical reactions are considered.

(b) Redox condition is controlled by HS^-/SO_4^{2-} and the precipitation/dissolution of calcite.
The redox controlled by HS-/SO_4 is assumed to keep the condition anoxic. In addition, the precipitation/dissolution reaction of calcite controls aqueous calcium concentration since calcite is a very common fracture filling.

(c) Consumption of dissolved oxygen in meteoric water by pyrite oxidation (Considering redox conditions controlled by HS^-/SO_4^{2-} and precipitation/dissolution of calcite)
Pyrite is oxidised when it contacts with dissolved oxygen in groundwater. Therefore, the following reaction is considered for oxic meteoric water:

$$FeS_2 + \frac{1}{2}H_2O + \frac{15}{4}O_2 \rightarrow Fe^{3+} + 2SO_4^{2-} + H^+$$

In this calculation, it is assumed that the meteoric water is saturated with dissolved oxygen in equilibrium with air and that all of the dissolved oxygen is consumed for the pyrite oxidation, producing Fe^{3+} and SO_4^{2-}.

(d) HCO_3 production caused by decomposition of organic material in meteoric water
(Considering redox condition controlled by HS^-/SO_4^{2-} and precipitation/dissolution of calcite)
The decomposition of organic material in the meteoric water is a most promising process for the production of HCO_3^-. In the calculation, 20mmol of HCO_3^- is assumed to be supplied by the decomposition of organic material.

(e) Cation exchange between Ca and Na
(Considering redox condition controlled by HS^-/SO_4^{2-} and precipitation/dissolution of calcite)
The following conditions related to cation exchange reactions are assumed; 1) the cation exchange reaction occurs on clay minerals, 2) the content of clay mineral is 20% and 3) the clay minerals within 0.1mm in depth from fracture surfaces participate in the reaction. The geochemical data related to the reaction is determined based on those of bentonite in the JNC report (1999).

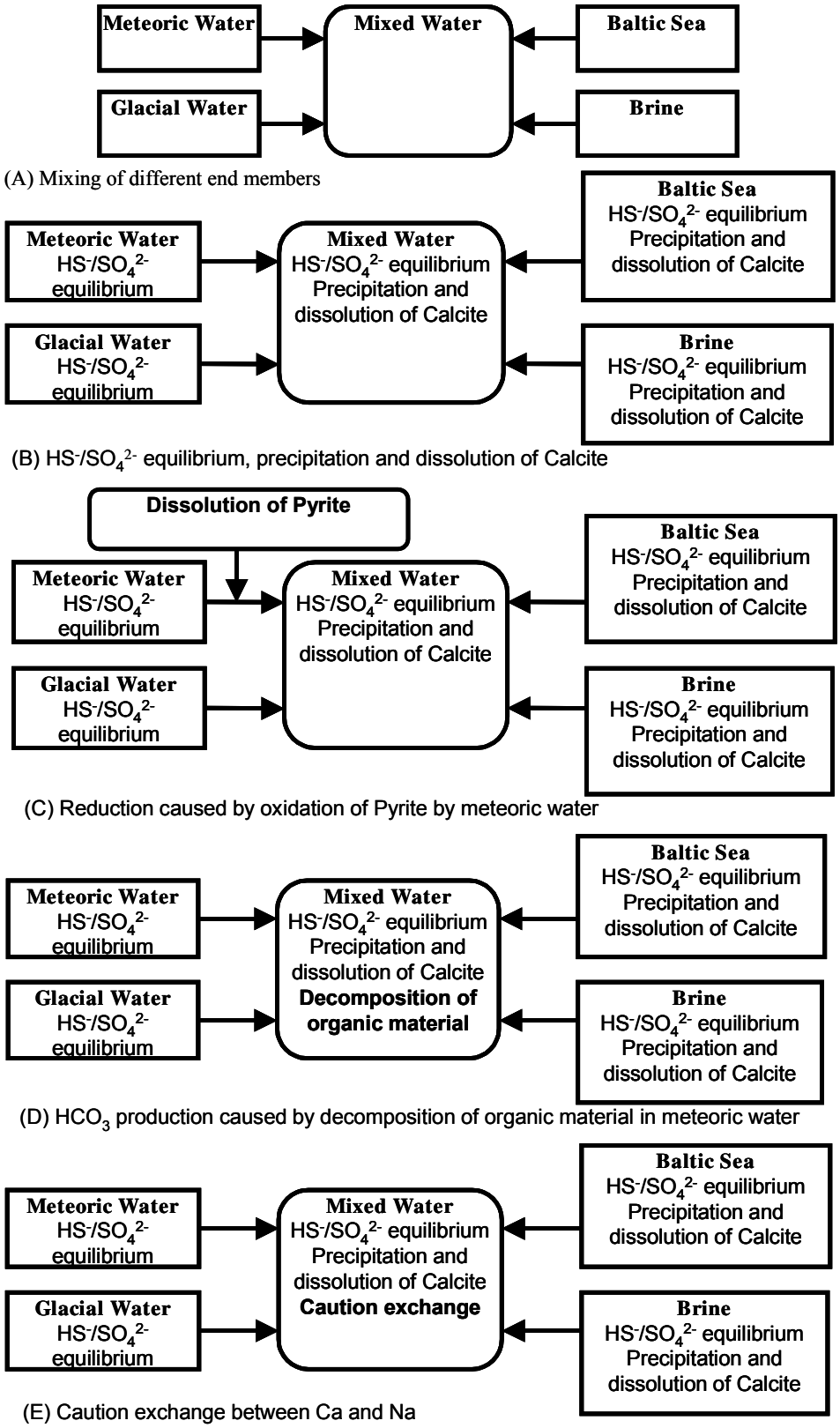

Figure 25. *Geochemical reaction models included in this study.*

7.6 Calculated results

The calculated results are shown in Figures 26 and 27. Figure 26 represents the predicted results based on the M3, whereas Figure 27 represents the predicted values ones based on the simulated results by FEGM/FERM (see the mixing proportion in Fig.19).

1) Decomposition of organic material is sensitive to the concentration of HCO_3^-. It indicates that the decomposition of organic material controls the HCO_3^- concentration. The measured concentration could be represented by considering this reaction at shallow part. Whereas the simulated HCO_3^- concentrations at KA2074A and KA2783A did not agree with the measured data, these is some possibility that it is caused by the consumption of organic materials at shallow part.

2) Cation exchange reactions affected the concentration of cations. By considering this reaction, the difference between measured and calculated concentration could decrease at the most of monitoring points.

3) The effects of the redox condition controlled by HS^-/SO_4^{2-}, the precipitation/dissolution of calcite, and the oxidation of pyrite were insignificant.

4) As shown in Figure 19, the mixing proportion of measured and simulated are quite different, in particular at KA2783, but they are not so different when the components are compared directly. Therefore, it may be difficult to identify the mixing proportion under high mixing conditions and considering the reactions.

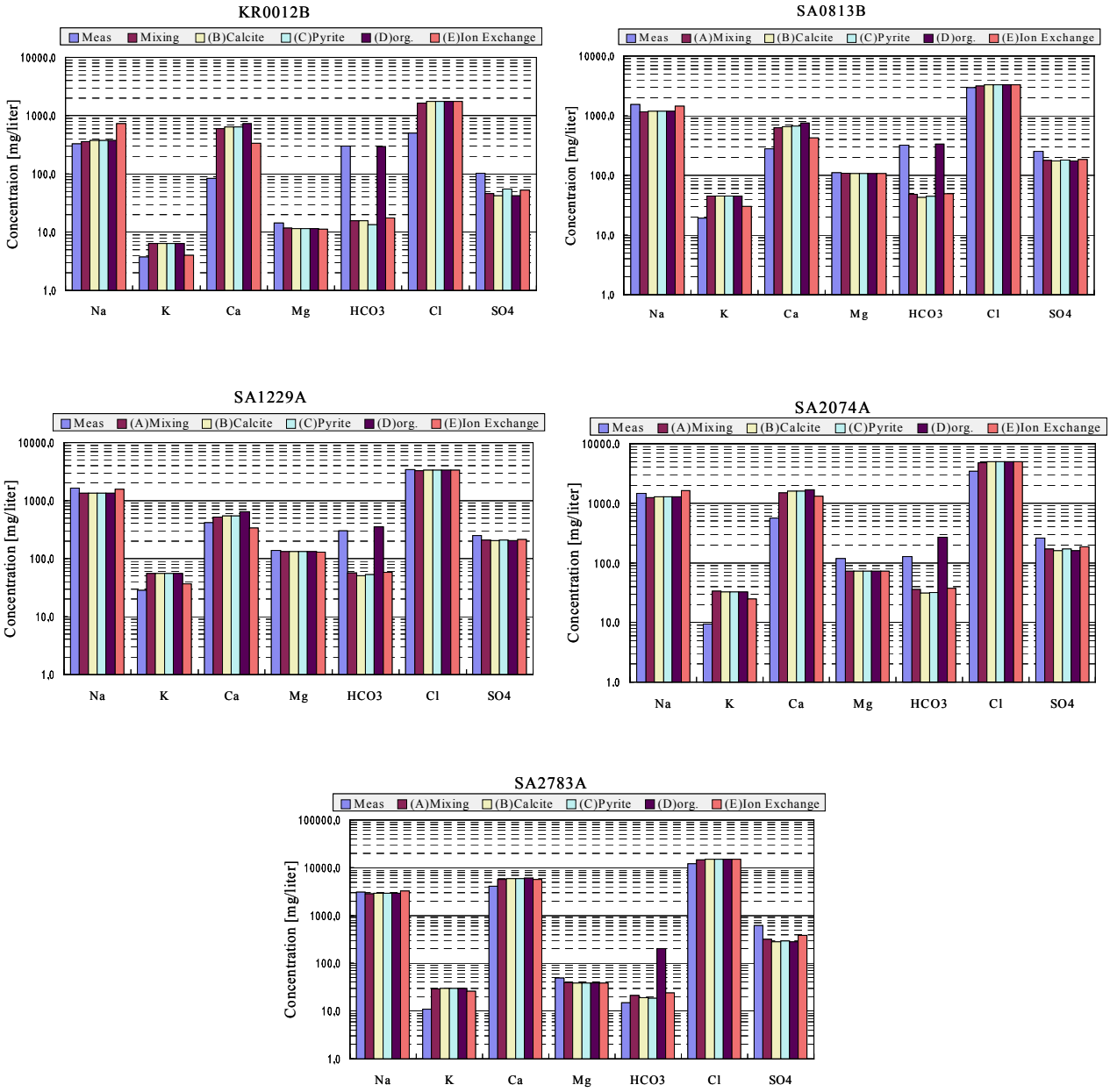

Figure 26. *Chemical concentrations based on reactions.*
(Based on the M3 model)

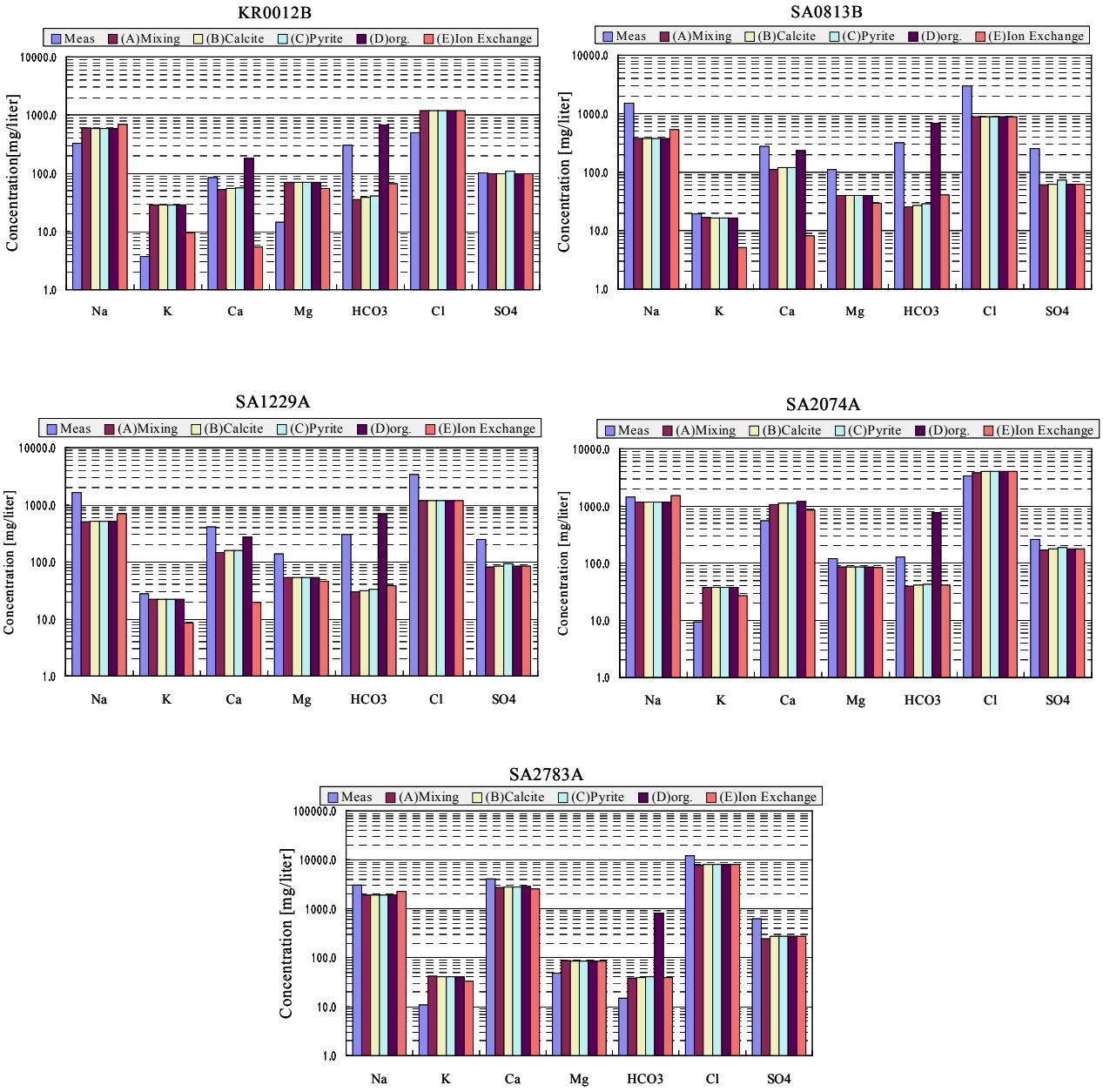

Figure 27. *Chemical concentrations based on reactions.*
(Based on FEGM/FERM)

8. Main results

The groundwater flow and geochemical distribution was simulated during tunnel construction around Äspö. The stability of selected geochemical components were investigated using PHREEQE.

Groundwater flow
Excluding modelling the grouting and skin effect around tunnel, the unsteady state of the groundwater flow was simulated, expelling the flux measured at the weirs from the tunnel section. Calibrations of transmissivities of the Hydraulic Conductor Domains (HCDs) were also performed.

In particular, the hydraulic conductivity of NNW-7 and the HRDs is valuable in simulating drawdowns. The HCDs crossing the spiral tunnel and shaft are important to evaluate drawdowns., e.g. NNW-1, NNW-2, NNW-4, NNW-7,NE-2. It is important to model the HRDs, because the hydraulic conductivity of the HRDs, although low, influence the drawdowns.

The progress of tunnel construction and the time series of drawdowns are quite useful to refine the hydrogeological model because these relationships are useful to clarify the impact and response. Drawdowns were roughly represented by properly representing the geometric relationship between tunnel, shaft, HCD and monitoring borehole section.

Since the simulated drawdowns represent the timing and amount of drawdown, the hydrogeological model is valid from the point of geometric and hydraulic properties.

Geochemical distribution
The geochemical distribution of selected chemical components was simulated on the basis of the results of Multivariate Mixing Mass balance (M3) calculations.

Since the replacement of groundwater occurred when the tunnel excavation passed the monitoring point, the groundwater movement is deduced by tunnel construction. The changes of mixing proportions are caused by changes in flow due to tunnel construction.

The main features of the calculated mixing proportions at the monitoring points are as follows:

- At the shallow part of the monitoring points located at the access tunnel, the groundwater simply flows from the top boundary to the tunnel as expected, and the groundwater tends to be replaced by fresh water, i.e. Baltic Sea water and Meteoric water, and the mixing proportion of old water, that is, Brine and Glacial water, will decrease. At the deeper part of the monitoring points which cross the HCDs, replacement by fresh water still occurs, but the old water proportions still remain as a few tens of percent.

- The simulated mixing portions of old waters (i.e. Glacial water and Brine water) and sum total of fresh waters (i.e. sum total of Baltic Sea water and Meteoric water) agreed with the results of M3, but the ratio of fresh water disagreed. Based on the simulated mixing proportions, the deeper part of the groundwater was replaced by Baltic Sea water rather than Meteoric water.

Further studies are needed to explain this inconsistency, for example, geochemical reactions, boundary conditions, local effect of sampling. However, the investigation focusing on the end-members is useful to understand the path of groundwater flow and the properties of the HCDs.

Helium transport
Concerning measured helium concentrations, the simulated helium concentrations are generally in good agreement with the measured concentrations. Since measured and simulated results reflect the hydraulic properties of the HCDs, it is a potentially useful method to verify the hydrogeological model.

Geochemical reactions
With regard to geochemical reaction modelling, some compositions are sensitive to reactions within the Äspö environment, especially HCO_3. Under such circumstances it is difficult to identify the mixing proportions under highly mixing conditions. Reactions and their impact on groundwater chemistry should be an area for further investigation.

Acknowledgements

The authors would like to thank Ingvar Rhen and John Smellie for their input to this report.

References

Brooks, A.N. and Hughes, T.J.R., 1982. Streamline Upwind Petrov-Galerkin formulation for convection dominated flow with particular emphasis on the impressible Navier-Stokes equations, Compt. Meths. Appl. Mech. Eng., 32, 199-259.

Brown, P.L. et al., 1991. HARPHRQ:A Geochemical speciation Program Based on PHREEQE - User Guide, UKAEA NSS/R188.

Cross, J.E. et al., 1990. HATCHES - a Thermodynamic Database and Management System, UKAEA NSS/R212.

Gurban, I., Laaksoharju, M., and Andersson, C., 1998. Influence of the tunnel construction on the groundwater chemistry at Äspö, Hydrochemical initial and boundary conditions: WP D1, WP D2, Part 2. Äspö HRL IPR-02-59, SKB, Stockholm, Sweden. (in press)

JNC: H12, 1999. Project to establish the scientific and technical basis for HLW disposal in Japan, Supporting Report 3, Safety Assessment of the Geological Disposal system.

Kawanishi, M. et al., 1994. Development of performance assessment method on natural barrier system for geological disposal of HLW(I): Analysis model for groundwater flow in fractured rocks, CRIEPI Rep. U93054 (in Japanese).

Kawanishi, M. et al., 1995. Development of performance assessment method on natural barrier system for geological disposal of HLW(II): Analysis model for thermal transport and radionuclide migration in fractured rock, CRIEPI Rep. U94053 (in Japanese).

Laaksoharju, M., Tullborg, E. L., Wikberg, P., Wallin, B., and Smellie, J., 1999. Hydrogeochemical conditions and evolution at the Äspö HRL, Sweden. Appl. Geochem. 14, 835-859.

Mahara, Y., Igarashi, T., Hasegawa, T., Miyakawa, K., Tanaka, Y., and Kiho, K., 2001. Dynamic changes in hydrogeochemical conditions caused by tunnel construction at Äspö Hard Rock Laboratory (HRL), Sweden., Appl. Geochem. 16, 291-315.

Rhen, I., Gustafson, G., Stanfors, R. and Wikberg, P., 1997. Äspö HRL – Geoscientific evaluation 1997/5, Models based on site characterization 1986-1995. SKB Tech. Rep. (TR-97-06), SKB, Stockholm, Sweden.

Torgersen, T. and Clarke, W. B., 1987. Helium accumulation in groundwater, III. Limits on helium transfer across the mantle-crust boundary beneath Australia and the magnitude of mantle degassing, Earth Planet. Sci. Lett. 84, 345-355.

Appendix 1: Questionnaire

MODELLING QUESTIONNAIRE FOR TASK 5, CRIEPI

worked October 1999

This is a Modelling Questionnaire prepared by SKB based on discussions within the Task Force group. It should be answered when reporting Task 5 in order to simplify the evaluation process of the modelling exercise. Preferably, include this response in an appendix to your forthcoming report.

1. SCOPE AND ISSUES

a) What was the purpose for your participation in Task 5?

Our purposes for participation in Task 5 are
to understand the site scale groundwater flow and solute transport.
to enhance the applicability of FEGM/FERM.

b) What issues did you wish to address through participation in Task 5?
The accuracy of the modelling results, how to understand the site scale groundwater flow and solute transport and how to calibrate

2. CONCEPTUAL MODEL AND DATA BASE

a) Please describe your models using the tables 1-3 in the appendix.
b) To what extent have you used the data sets delivered? Please fill in Table 4 in the appendix.
c) Specify more exactly what data in the data sets you actually used? Please fill in "Comments" in Table 4
d) What additional data did you use if any and what assumptions were made to fill in data not provided in the Data Distributions but required by your model? Please add in the last part of Table 4.
e) Which processes are the most significant for the situation at the Äspö site during the simulation period?

Tunnel construction and tunnel pass the hydraulic conductor domains

3. MODEL GEOMETRY/STRUCTURAL MODEL

a) How did you geometrically represent the ÄSPÖ site and its features/zones?

Modelling area was represented by hex element and tunnel was represented by line elements. The hydraulic conductor domains were represented using Smeared Fracture Model; the material properties intersected by hydraulic conductors are assigned as volumetric averaging value.
The topology of ÄSPÖ is neglected, but the area of ÄSPÖ is modelled as the rainfall of groundwater flow. The accuracy of representation depends on spatial discrimination by finite element.

b) Which features were considered the most significant for the understanding of flow and transport in the ÄSPÖ site, and why?

Hydraulic conductors defined by SR97 were considered in modelling. These fracture zones are important to evaluate groundwater flow and solute transport.
In this modelling we focus on comparing measured with calculated, so it is not well understand which feature is most significant from the view of site scale groundwater flow and solute transport. But from the view of comparing between measured and calculated, the transmissivity of NNW-7 is the most sensitive to the calculated drawdowns.

c) Motivate selected numerical discretization in relation to used values of correlation length and/or dispersion length.

4a. MATERIAL PROPERTIES - HYDROGEOLOGY

a) How did you represent the material properties in the hydraulic units used to represent the ÄSPÖ SITE?
The material properties are divided into two categories. One is rock mass domain called HRD, the others are hydraulic conductor domain called HCD. Spatial distribution and deep-dependency of hydraulic permeability were neglect for HRD, and variation of hydraulic transmissivity for HCD were neglect.
b) What is the basis for your assumptions regarding material properties?
It is difficult and complex to consider the spatial distribution and variation of hydraulic permeability.
Not considered property of unsaturated flow
c) Which assumptions were the most significant, and why?
Neglecting some conductive fractures in the rock mass domain
This neglecting will be important at high drawdown part.

4b. CHEMICAL REACTIONS - HYDROCHEMISTRY

a) What chemical reactions did you include?
The following reactions are included,
1) HCO_3 production caused by decomposition of organic material in meteoric water
2) Consumption of dissolved oxygen in meteoric water by pyrite oxidation
3) Precipitation and dissolution of calcite
4) Cation exchange by clay minerals
5) Oxidation-reduction between HS^- and $SO4^{2-}$
b) What is the basis for your assumptions regarding the chosen chemical reactions?
The chosen chemical reactions are based on 'Groundwater reaction to consider within the Task 5 modeling'.
c) Which reactions were the most significant, and why?
The following reactions are significant,
Decomposition of organic materia control HCO^{3-} concentration
Caution exchange reactions affected the concentration of cautions

5a. BOUNDARY CONDITIONS FOR HYDROGEOLOGICAL MODEL

a) What boundary conditions were used in the modelling of the ÄSPÖ site tests?
Prescribed flux at weir in the tunnel
Prescribed pressure at the top and the side of modelling area
No flux at bottom of modelling area and constant flux at ÄSPÖ
Prescribed concentration at the top and side boundary of modelling area were used, and the values of boundary were calculated from provided data set.

b) What was the basis for your assumptions regarding boundary conditions?
It is difficult to quantify the skin effect of tunnel, so prescribed flux at weir of tunnel are used.
Side and bottom boundaries are not influenced to the calculation result so much, so above mentioned boundaries were assumed.

c) Which assumptions were the most significant, and why?
Initial and boundary condition for solute transport
The mixing portions of four end-members located at the upper part of the tunnel depend on boundary value, because the transport time is quit shorter than simulation time.

5b. BOUNDARY/INITIAL CONDITIONS FOR HYDROCHEMICAL MODEL

a) What boundary conditions were used in the modelling of the ÄSPÖ site tests?
Equibirium geochemical reactions calculated by HARPHRQ were considered for the mixing rates calculated by solute transport model, so the evaluation coupling geohydrogical and geochemical were not conducted.
b) What was the basis for your assumptions regarding boundary conditions?

c) Which assumptions were the most significant, and why?
Decomposition of organic material and caution exchange
Because they are sensitive to the results

6. MODEL CALIBRATION

a) To what extent did you calibrate your model on the provided hydraulic information? (Steady state and transient hydraulic head etc.)
The model calibration were performed for transient state using time series of drawdowns.
To what extent did you calibrate your model on the provided "transport data"? (Breakthrough curves etc.)
No calibration

b) To what extent did you calibrate your model on the provided hydrochemical data? (Mixing ratios; density/salinity etc.)
No calibration

c) What parameters did you vary?
Transmissivity of fracture and hydraulic permeability of rock mass

d) Which parameters were the most significant, and why?
Transmissivity of fracture

e) Compare the calibrated model parameters with the initial database - comments?
Most of hydraulic parameters were well defined to represent the change of drawdowns.

7. SENSITIVITY ANALYSIS

Identify the sensitivity in your model output to:

a) the discretization used
Time discretization is very sensitive to the result. Time step should be smaller than 15days to get the result in this calculation.
The effect of spatial discretization is unknown.

b) the transmissivity/hydraulic conductivity (distribution) used
Sensitive

c) transport parameters used
Not conducted

d) chemical mixing parameters used
Not conducted

e) chemical reaction parameters used
Not conducted

8. LESSONS LEARNED

a) Given your experience in implementing and modelling the ÄSPÖ site, what changes do you recommend with regards to:

- Experimental site characterisation?
More time series of concentration at certain point
- Presentation of characterisation data?

- Performance measures and presentation formats?
More simple geochemical distribution should be simulated as performance measurement.

b) What additional site-specific data would be required to make a more reliable prediction of the tracer experiments?
More typical distribution of solute and more time series

c) What conclusions can be made regarding your conceptual model utilised for the exercise?
The groundwater flow modelling (ex. Response of drawdown)
The groundwater flow was well represented using aforementioned conceptual model.

d) What additional generic research results are required to improve the ability to carry out predictive modelling of transport on the site scale?
.Paleohydrogy using stable isotope

9. RESOLUTION OF ISSUES AND UNCERTAINTIES

a) What inferences did you make regarding the descriptive structural-hydraulic model on the site scale for the ÄSPÖ site?

The location of NNW-7 could be located little bit close to KAS02

b) What inference did you make regarding the active hydochemical processes, hydrochemical data provided and the hydrochemical changes calculated?

The groundwater under Aspo could be replaced by Baltic water.

c) What issues did your model application resolve?

The application of calculation method is good for compiling the hydrogeological and hydrochemical information. For evaluating the geochemical distribution, more interpretations are needed to understand the groundwater flow.

d) What additional issues were raised by the model application?

It is difficult to calibrate the model using hydrochemical data, because the distribution of hydrochemical spices are not well known the initial and boundary condition comparing the groundwater flow. To get more effective results, selecting the hydrochemical spices that has more acceptable and distinctive features are necessary.

10. INTEGRATION OF THE HYDOGEOLOGICAL AND HYDROCHEMICAL MODELLING

a) How did you integrate the hydrogeological and hydro chemical work?

The inconsistency between hydrogeological and hydrochemical still remain, but it may be useful to consider both on modelling.

b) How can the integration of the hydrogeological and hydrochemical work be improved?

c) Hydrogeologist: How has the hydrochemistry contributed to your understanding of the hydrogeology around the Äspö site?

To calculate the geochemical distribution is good for understanding the groundwater flow. However there are big inconsistency between measured data and calculated data.

d) Hydrochemist: How has the hydrogeology contributed to your understanding of the hydrochemistry around the Äspö site?

Table 1 Description of model for water flow calculations

TOPIC	Example	Our Model
Type of model	Stochastic continuum model	Determistic continuum model
Process description	Darcy´s flow including density driven flow. (Transport equation for salinity is used for calculation of the density)	Darcy's flow
Geometric framework and parameters	Model size: 1.8x1.8x1 km^3 . Deterministic features: All deterministic features provided in the data set. Rock outside the deterministic features modelled as stochastic continuum.	Model size: 2.0x2.5x1 km^3 . Easting 1000-3000m, Northing 5500-8000m, 0 - -1000m in depth at Aspo coodinate Determistic features: All except for regional structure, ex. SFZ03, SFZ12. Rock outside the deterministic features modelled as determistic continuum.
Material properties and hydrological properties	Deterministic features: Transmissivity (T), Storativity(S) Rock outside deterministic features: Hydraulic conductivity(K), Specific storage (Ss)	Deterministic features: Transmissivity (T) Rock outside deterministic features: Hydraulic conductivity(K), Specific storage (Ss) is same in the modelling area
Spatial assignment method	Deterministic features: Constant within each feature (T,S). No changes due to calibration. Rock outside deterministic features: (K,Ss) lognormal distribution with correlation length xx. Mean, standard deviation and correlation based on calibration of the model	Deterministic features: Constant within each feature (T). Transmissivity of NNW-7 changes twice value due to calibration, Transmissivity based on Table A2-7 and A2-8, TR97-06 Rock outside deterministic features: Unity value Before calibration, 1.5e-9m/s (3m-scale hydraulic permeability test) After calibration, 6.0e-9 m/s (3m-scale hydraulic permeability test)
Boundary conditions	Surface: Constant flux. Sea: Constant head Vertical-North: Fixed pressure based on vertical salinity distribution. Vertical-East: Fixed pressure based on vertical salinity distribution. Vertical-South: Fixed pressure based on vertical salinity distribution. Vertical-West: Fixed pressure based on vertical salinity distribution. Bottom: No flux. Linear change by time based regional simulations for undisturbed conditions and with Äspö tunnel present.	Surface: Constant flux in Aspo, Constant head in others that mean sea and island, ex. Laxmar, Halo and Mjalen. Side: Fixed pressure based on hydrostatic pressure. Bottom: No flux. Tunnel: time variable flux boundary, tunnel gain is expressed by hydraulic permeability chenge at line element.
Numerical tool	PHOENICS	**FEGM**/FERM
Numerical method	Finite volume method	Finite element method
Output parameters	Head, flow and salinity field.	Head, Darcy's velocity

Table 2 Description of model for tracer transport calculations

TOPIC	EXAMPLE	Our model
Type of model	Stochastic continuum model	Determistic continum mode
Process description	Advection and diffusion, spreading due to spatially variable velocity and molecular diffusion.	Advection and dispersion
Geometric framework and parameters	Model size: 1.8x1.8x1 km^3 . Deterministic features: All deterministic features provided in the data set. Rock outside the deterministic features modelled as stochastic continuum.	Model size: 2.0x2.5x1 km^3 . Easting 1000-3000m, Northing 5500-8000m, 0 - -1000m in depth at Aspo coodinate Determistic features: All except for ???, which Rock outside the deterministic features modelled as determistic continuum.
Material properties	Flow porosity (ne)	Flow prosity (ne) calculated from the experimetal relationship between hydraulic permeability and flow prosity. cf. Eq(8-8), pp.399, TR97-06.
Spatial assignment method	ne based on hydraulic conductivity value (TR 97-06) for each cell in model, including deterministic features and rock outside these features.	Flow prosity (ne) calculated from the experimetal relationship between hydraulic permeability and flow prosity. cf. Eq(8-8), pp.399, TR97-06 for each element.
Boundary conditions	Mixing ratios for endmembers as provided as initial conditions in data sets.	Mixing ratios for endmembers as provided as initial conditions in data sets.
Numerical tool	PHOENICS	FEGM/**FERM**
Numerical method	Particle tracking method or tracking components by solving the advection/diffusion equation for each component	Finite element method with upwinding method called Petrov-Galerkin method
Output parameters	Breakthrough curves	Concentration

Table 3 Description of model for chemical reactions calculations

TOPIC	EXAMPLE	Our model
Type of model	xxx	Equilibrium geochemical reaction
Process description	Mixing. Reactions: Xx, Yy,Zz,Dd…..	Mixing. Reaction: 1) HCO3 production caused by organic decomposition 2)Reduction(deoxidation) caused by Prrite dissolution 3)Calcite dissolution and sedimentation 4)Caution exchange for clay minerals 5)oxidation-reduction for $HS^-/SO4^{2-}$
Geometric framework and parameters	Modelling reactions within one fracture zone, NE-1.	
Reaction parameters	Xx: a=ff, b=gg,… Yy: c=. Zz: d=...	
Spatial distribution of reactions assumed	Xx: seafloor sediments Yz: Bedrock below sea, superficial Dd: Bedrock ground surface, superficial Yz: Bedrock below sea, at depth Zz: Bedrock ground surface, at depth Yy, Zz: near tunnel	
Boundary/initial conditions for the reactions	Xx: aaa… Yy: bbb…	Calculated mixing portion from FEGM/FERM
Numerical tool	Phreeque	Phreeque HARPHRQ, cf P.L. Brown et al.:HARPHRQ, UKAEA NSS/R188 (1991) HATCHES database NEA Release, cf. J.E. Cross et al.:HATCHES NSS/R212(1990)
Numerical method	xx	
Output parameters	xx	Amount of geochemical spices

Table 4a Summary of data usage

Data del. No	Data	Importance of data (see notes)	Comment
1	Hydrochemical data 1	-	
1a	Surface bore holes- undisturbed conditions, Äspö-Laxemar		
1b	Surface bore holes- disturbed conditions (by tunnel excavation), Äspö		
1c	Surface bore holes- undisturbed conditions, Ävrö		
1d	Surface bore holes- sampled during drilling, Äspö		
1e	Data related to the Redox experiment		
1f	Tunnel and tunnel bore holes- disturbed conditions		
2	Hydogeological data 1		
2a1	Annual mean air temperature	-	
2a2	Annual mean precipitation	X	
2a3	Annual mean evapotranspiration	X	Predicting infiltration rate
2b1	Tunnel front position by time	**M**	Boundary condition at the tunnel
2b2	Shaft position by time	**M**	Boundary condition at the shaft
2c1	Geometry of main tunnel	**M**	Described as line element in the model
2c2	Geometry of shafts	**M**	Described as line element in the model
2d	Hydrochemistry at weirs (Cloride, pH, Electrical conductivity, period: July 1993- Aug 1993)	-	
2e	Geometry of the deterministic large hydraulic features (Most of them are fracture zones)	**M**	

Table 4b Summary of data usage

Data del. No	Data	Importance of data (see notes)	Comment
3	Hydrogeological data 2		
3a	Monthly mean flow rates measured at weirs. Tunnel section 0-2900m, period May 1991 – January 1994	**M**	Boundary condition at the tunnel
3b	Piezometric levels for period June 1st 1991 – May 21st 1993. Values with 30 days interval (Task 3 data set)	X	
3c	Salinity levels in bore hole sections for period -Sept 1993. (Task 3 data set)	-	
3d	Undisturbed piezometric levels	-	
3e	Co-ordinates for bore hole sections	**P**	
3f	Piezometric levels for period July 1st 1990 – January 24st 1994. Daily values.	**P**	Only use at calibration
4	Hydochemical data 2	-	
4a	Chemical components, mixing proportions and deviations for all bore hole sections used in the M3 calculations		
4b	Bore holes with time series, > 3 samples (part of 4a)		
4c	Bore holes sections interpreted to intersect deterministic large hydraulic features (Most of them are fracture zones) (part of 4a)		
4d	Chemical components, mixing proportions and deviations. Grid data based on interpolation. Undisturbed conditions		
4e	Chemical components, mixing proportions and deviations. Grid data based on interpolation. Disturbed conditions (by tunnel excavation)		
4f	Boundary and initial conditions. Chemical components, mixing proportions and deviations (1989). Grid data for vertical boundaries based on interpolation. Undisturbed conditions		
4g	Boundary conditions after tunnel construction (1996) Chemical components, mixing proportions and deviations. Grid data for vertical boundaries based on interpolation. Disturbed conditions (by tunnel excavation)		

Table 4c Summary of data usage

Data del. No	Data	Importance of data (see notes)	Comment
5	Geographic data 1		
5a	Äspö coast line	**M**	Boundary condition
5b	Topography of Äspö and the nearby surroundings	-	
6	Hydro tests and tracer tests	-	
6a	Large scale interference tests (19 tests)		
6b	Long time pump and tracer test, LPT2	p	Only use at preliminary calculation
7	Hydochemical data 3, update of data delivery 4 based on new endmembers. Recommended to be used instead of 4.	**P**	
7a	Chemical components, mixing proportions and deviations for all bore hole sections used in the M3 calculations	**P**	
7b	Bore holes with time series, > 3 samples (part of 7a)		
7c	Bore holes sections interpreted to intersect deterministic large hydraulic features (Most of them are fracture zones) (part of 7a)		
7d	Chemical components, mixing proportions and deviations. Grid data based on interpolation. Undisturbed conditions		
7e	Chemical components, mixing proportions and deviations. Grid data based on interpolation. Disturbed conditions (by tunnel excavation)		
7f	Boundary and initial conditions. Chemical components, mixing proportions and deviations (1989). Grid data for vertical boundaries based on interpolation. Undisturbed conditions	**P**	Boundary condition for solute transport
7g	Boundary conditions after tunnel construction (1996) Chemical components, mixing proportions and deviations. Grid data for vertical boundaries based on interpolation. Disturbed conditions (by tunnel excavation)	p	

Table 4d Summary of data usage

Data del. No	Data	Importance of data (see notes)	Comment
8	Performance measures and reporting 1	**P**	
8a	Performance measures	**P**	
8b	Suggested control points. 6 points in tunnel section 0-2900m and 3 point in tunnel section 2900-3600m.	P	
8c	Suggested flowchart for illustration of modelling	-	
9	Hydrogeological data 3	**M**	
9a	Monthly mean flow rates measured at weirs. Tunnel section 0-3600m, period: May 1991- Dec 1996.	**M**	
10	Geographic data 2	-	
10a	Topography of Äspö and the nearby surroundings (larger area than 5b)		
10b	Co-ordinates for wetlands		
10c	Co-ordinates for lakes		
10d	Co-ordinates for catchments		
10e	Co-ordinates for streams		
10f	Co-ordinate transformation Äspö system- RAK		
11	Boundary and initial conditions	-	
11a	Pressure before tunnel construction, from the regional SKB model (TR 97-09)		
11b	Salinity before tunnel construction, from the regional SKB model (TR 97-09)		
11c	Pressure after tunnel construction, from the regional SKB model (TR 97-09)		
11d	Salinity after tunnel construction, from the regional SKB model (TR 97-09)		

Table 4e Summary of data usage

Data del. No	Data	Importance of data (see notes)	Comment
12	Performance measures and reporting 2	-	
12a	Suggested control points. 6 points in tunnel section 0-2900m and 3 point in tunnel section 2900-3600m (same as 8b) and 2 outside the tunnel.		
13	Transport parameters compiled	X	
13a	LPT2 tracer tests	X	
13b	Tracer test during passage of fracture zone NE-1	X	
13c	Redox tracer tests		
13d	TRUE-1 tracer tests		
14	Hydrochemical data 4	X	
14a	Groundwater reactions to consider within TASK5 modelling (Description of how M3 calculates the contribution of reactions and identifying dominating reactions based on the M3 calculations.		
15	Co-ordinates for the test sections defining the control points	-	
16	Co-ordinates for bore holes drilled from the tunnel	-	

Table 4f Summary of data usage

Data del. No	Data	Importance of data (see notes)	Comment
17	Hydogeological data - prediction period		
17a	Hydrochemistry at weirs (Cloride, pH, Electrical conductivity, period: July 1993- Dec 1995)		
17b	Piezometric levels for period July 1st 1990 – Dec 1996. Daily values.		
18	Hydochemical data - prediction period.		
18a	Chemical components, mixing proportions and deviations for all bore hole sections used in the M3 calculations. Data for tunnel section 2900-3600m.		
18b	Bore holes with time series, > 3 samples (part of 18a)		
18c	Bore holes sections interpreted to intersect deterministic large hydraulic features (Most of them are fracture zones) (part of 18a)		
	Other data (part of data to Task 1, 3 and 4)		
	Transmissivity of fracture zone and Hydraulic permeaility of host rock were estimated from Model96		
	Effective procity		
	Dispersion length		

P = data of great importance for quantitative estimation of model parameters
p = data of less importance for quantitative estimation of model parameters
M = data of great importance used qualitatively for setting up model
m = data of less importance used qualitatively for setting up model
X = data useful as general background information
- = data not used